Gersonde, R., Hodell, D.A., Blum, P., et al., 1999
Proceedings of the Ocean Drilling Program, Initial Reports Volume 177

2. EXPLANATORY NOTES[1]

Shipboard Scientific Party[2]

INTRODUCTION

In this chapter, we have assembled information that will help the reader understand the procedures of shipboard data acquisition and our preliminary conclusions. This information concerns only shipboard operations and analyses described in the site chapters of the Leg 177 *Initial Reports* volume of the *Proceedings of the Ocean Drilling Program*. Methods used by various investigators for shore-based analyses of Leg 177 data will be described in individual scientific contributions published elsewhere.

Drilling Operations

Two coring systems were used during Leg 177: the advanced hydraulic piston corer (APC) and the extended core barrel (XCB). Either of these systems was applied to maximize core recovery in the lithology being drilled. Each cored interval was about 9.5 m long, which is the length of a core barrel. In some cases, the drill string was "washed ahead" without recovering sediments to advance the drill bit to a target depth where core recovery needed to resume. Drilling systems and their characteristics, such as drilling-related deformation, are summarized in the "Explanatory Notes" chapters of previous *Initial Reports* volumes. The Leg 139 *Initial Reports* volume (Davis, Mottl, Fisher, et al., 1992) includes a particularly detailed description.

Drilled intervals are referred to in meters below rig floor (mbrf), which are measured from the kelly bushing on the rig floor to the bottom of the drill pipe, and meters below seafloor (mbsf), which are calculated by subtracting the seafloor depth in mbrf. In the case where sediments of substantial thickness cover the seafloor (as at all sites drilled during Leg 177), the mbrf depth of the seafloor is determined with a mudline core, assuming 100% recovery for the cored interval in

[1]Examples of how to reference the whole or part of this volume.
[2]Shipboard Scientific Party addresses.

Ms 177IR-102

the first core. Water depth is calculated by subtracting the distance from the rig floor kelly bushing to the sea level from the mudline measurement in mbrf. This water depth usually differs from precision depth recorder measurements by a few meters. The mbsf depths of core tops are calculated by subtracting the seafloor depth in mbrf from the core-top depth in mbrf. The core-top datums from the driller are the ultimate depth reference for any further depth calculation procedures.

Curatorial Procedures and Sample Depth Calculations

Numbering of sites, holes, cores, and samples follows the standard Ocean Drilling Program (ODP) procedure. A full curatorial identifier for a sample consists of the following information: leg, site, hole, core number, core type, section number, and interval in centimeters measured from the top of the core section. For example, a sample identification of "177-1088A-1H-1, 10–12 cm" would represent a sample removed from the interval between 10 and 12 cm below the top of Section 1, Core 1H (H designates that this core was taken with the APC system) of Hole 1088A cored during Leg 177.

Cored intervals are also referred to in curatorial meters below seafloor (mbsf). The mbsf of a sample is calculated by adding the depth of the sample below the section top and the lengths of all higher sections in the core to the core-top datum measured with the drill string. A sediment core from less than a few hundred meters below seafloor expands upon recovery (typically 10% in the upper 300 m) so that its length does not match the drilled interval it originates from. In addition, there is typically a coring gap between cores, as shown by composite depth construction (see below). Thus, a discrepancy exists between the drilling mbsf and the curatorial mbsf. For instance, the curatorial mbsf of a sample taken from the bottom of a core may be larger than that of a sample taken from the top of the subsequent core, which creates a stratigraphic dilemma. To avoid this problem, multiple holes (typically three to five) were drilled at a site to construct a continuous composite section. This resulted in a "meters composite depth" (mcd) scale for each site that accommodates core expansion and drilling gaps through interhole correlation using closely spaced measurements of core physical properties (see **"Composite Depths,"** p. 3).

Core Handling and Analysis

General core handling procedures, described in previous *Initial Reports* volumes and the Shipboard Scientist's Handbook, are summarized here. As soon as cores arrived on deck, core-catcher (CC) samples were taken for biostratigraphic analysis. After the core was cut in sections, whole-round samples were taken for shipboard interstitial water analysis. In addition, headspace gas samples were immediately bored from the ends of cut sections and sealed in glass vials for light hydrocarbon analysis.

Before splitting, whole-round core sections were run through the multisensor track (MST) and thermal conductivity measurements were taken. The cores were then split into working and archive halves, from bottom to top, so investigators should be aware that older material could have been transported upward on the split face of each section. The working half of each core was sampled for both shipboard analysis, such as physical properties, carbonate, and bulk X-ray diffraction (XRD) mineralogy, and shore-based studies. Shipboard sampling was kept at a

minimum during Leg 177 to allow construction of a detailed sampling plan after the composite section was built. The archive-half sections were passed through the cryogenic magnetometer and described visually and by means of smear slides. The archive half was then photographed with both black-and-white and color film, a whole core at a time, and close-up photographs were taken of particular features for illustrations in the site reports, as requested by individual scientists. The working half was analyzed using an automated color reflectance scanning system.

Both halves of the core were then put into labeled plastic tubes, sealed, and transferred to cold-storage space aboard the ship. At the end of the leg, the cores were transferred from the ship into refrigerated trucks and were shipped to the ODP Bremen Core Repository for cold storage.

COMPOSITE DEPTHS

The recovery of complete sedimentary sections within APC-cored intervals was crucial to the paleoceanographic objectives of Leg 177. Drilling of multiple holes at each site ensured that intervals missing from one hole as a result of recovery gaps were recovered in an adjacent hole. During Leg 177, as with previous ODP legs, the continuity of the recovered section was confirmed by composite depth sections developed for all multihole sites. The methods used during Leg 177 were similar to those used to construct composite depth sections during Leg 138 (Hagelberg et al., 1992), Leg 154 (Curry, Shackleton, et al., 1995), Leg 162 (Jansen, Raymo, Blum, et al., 1996), and Leg 167 (Lyle, Koizumi, Richter, et al., 1997).

At each site, closely spaced (2- to 4-cm interval) measurements of magnetic susceptibility and gamma-ray attenuation (GRA) wet bulk density were made using the MST soon after the core sections had equilibrated to room temperature. These measurements were entered into the shipboard database and minimally processed. In addition, measurements of spectral reflectance were made at 2- to 8-cm resolution on the split cores (see **"Physical Properties,"** p. 21). Magnetic susceptibility, spectral reflectance in the 650–700 nm band, and GRA bulk density measurements from each hole were compared to determine if coring offsets were maintained between holes. Integration of at least two different physical properties allowed hole-to-hole correlations to be made with greater confidence than would be possible with only a single data set.

Hole-to-hole correlations were made using interactive software developed specifically for this task. We used a software package ("Splicer") for Unix platforms that was developed at the Lamont-Doherty Earth Observatory Borehole Research Group (LDEO-BRG) and that was patterned after the Leg 138 correlation software. Corresponding features in data sets from adjacent holes were aligned using graphical and mathematical cross-correlations by an iterative process. Features were aligned by adjusting the mbsf coring depths, measured from the length of advanced drill string, on a core-by-core basis. No depth adjustments were made within a core. The resulting adjusted depth scale is the mcd scale.

The composite depth section for each site is presented in tabular form in the "Chronostratigraphy" section of each site chapter. For each section in each core, the depth adjustment required to convert from the

mbsf depth scale to the mcd scale is given. The last two columns in each table give, for each section, the cumulative depth offset added to the ODP mbsf curatorial sub-bottom depth and the composite depth, respectively. The depth-offset column facilitates conversion of sample depths that are recorded in ODP mbsf curatorial sub-bottom depth to composite depth. By adding the amount of offset listed to the depth in mbsf of a sample taken in a particular core, the equivalent depth in mcd is obtained.

Adjustments to the shipboard mbsf depth scale are required for several reasons (see short summaries in Ruddiman et al., 1987; Farrell and Janecek, 1991; Hagelberg et al., 1992, 1995). Rebound of the sediment following core recovery causes the cored sedimentary sequence to be expanded relative to the drilled interval. In addition, other factors, including random variations in ship motion and heave, can affect the "true" in situ depth of each core by introducing errors. Even between successive cores having nominally 100% or greater recovery, portions of the sedimentary sequence are usually missing. As a result, the mcd scale expands downhole relative to the mbsf scale, typically on the order of 10%.

The need for a composite section to verify stratigraphic continuity is illustrated in Figure **F1**. On the left panel, magnetic susceptibility from three holes at Site 1090 is shown on the mbsf depth scale. On the right panel, the same records are shown after depth-scale adjustment so that correlative features are aligned.

The correlation of lithologic parameters between multiple holes and associated depth adjustments for individual cores were optimized in such a way that a single record could be sampled from the aligned cores without any additional depth scale changes. Where the amount of offset necessary to align features was ambiguous or imprecise for all lithologic parameters, or where multiple hole data were unavailable, no additional depth adjustments were made. In these cases, the total amount of offset between mbsf depth and mcd is equal to the cumulative offset from the overlying cores. The composite depth section extends only to the base of multiple cored intervals, typically the APC intervals at Sites 1088 through 1094. Below the multiple cored intervals, cores were appended using the offset of the last core within the composite record to convert mbsf to mcd.

For each site, after the composite section was constructed, a representative record was assembled. Because the missing intervals between successive cores in the sedimentary sequence could be identified, it was possible to patch in these missing intervals with data from adjacent holes. The resulting "splice" provides a single representative record of each lithologic parameter (i.e., magnetic susceptibility, color reflectance, natural gamma, and GRA bulk density) for a given site. Additionally, these single records are ideally suited to serve as sampling schemes for paleoceanographic studies.

Splice tie points were made between adjacent holes at identifiable, highly correlated features. However, because there is considerable stretching and/or compression in many sections relative to the same sedimentary interval in adjacent holes, the exact length of the splice depends on which intervals of core were selected to build it. Each splice was constructed by beginning at the mudline at the top of the composite section and working downward. An example is given in Figure **F2**. Tables that provide the tie points for construction of the spliced records are presented in each site chapter (see "Chronostratigraphy" sections).

F1. Magnetic susceptibility records from Site 1090 plotted at mbsf and mcd scales, **p. 35.**

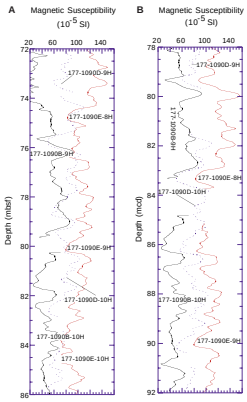

F2. Spliced magnetic susceptibility record from Site 1090, **p. 36.**

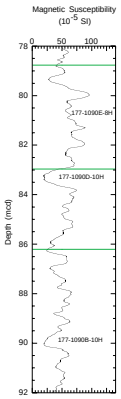

Intervals were chosen for the splice such that section continuity was maintained while disturbed intervals were avoided.

By identifying intervals where features present in multiple holes were most highly correlated, it was possible to construct a spliced record that avoided duplication or omission of any individual features or cycles. Splice tie points always connect features with exactly the same composite depths. As a result, the final alignment of the adjacent holes could be slightly different from the one giving the best overall visual or quantitative hole-to-hole correlation. Further adjustments to the composite depth section by expanding and compressing the depth scale within individual core intervals will be conducted postcruise to align all features exactly.

LITHOSTRATIGRAPHY

Classification of Sediments and Sedimentary Rocks

We have adopted the classification procedures suggested by Mazzullo et al. (1988) as modified by Leg 113 shipboard sedimentologists (Shipboard Scientific Party, 1988). According to Mazzullo's classification scheme, sediments encountered at the Leg 177 sites are granular sediments consisting of pelagic, siliciclastic, and volcaniclastic particles. Pelagic particles are defined as bioclastic grains composed of the skeletal remains of open-marine calcareous and siliceous microfauna and microflora derived from foraminifers, nannofossils, diatoms, and radiolarians as well as subordinate sponge spicules and silicoflagellates. The siliciclastic component consists of mineral and rock fragments that originated from igneous, sedimentary, and metamorphic rocks. In some recovered sediment cores, greenish brown glass shards were identified as volcaniclastic components that may occur as dispersed sand-sized particles in the host sediment or may form individual tephra beds.

We used the relative proportions of biogenic and siliciclastic components to define the major lithologic classes. Biogenic ("pelagic") sediment is composed of ≥50% biogenic grains, and siliciclastic deposits are composed of >50% siliciclastic grains. We modified the Mazzullo et al. (1988) terminology to avoid the designation of "mixed sediments" that includes biogenic and siliciclastic components in the range between 40% and 60%. We also define "mud" as the sum of silt and clay.

Descriptive Terminology: Principal Names

The principal name of biogenic sediments and sedimentary rocks relates to the chemical composition of the major component and the degree of compaction. The following names are used:

1. Ooze: unconsolidated calcareous and/or siliceous biogenic sediments.
2. Chalk: friable biogenic sediment composed predominantly of calcareous biogenic grains.
3. Chert: indurated biogenic sediment composed predominately of siliceous biogenic grains.

For siliciclastic sediments, the principal name describes the texture and is assigned according to the following guidelines:

1. The Udden-Wentworth grain-size scale (Wentworth, 1922) defines the grain-size ranges and the names of the textural groups (gravel, sand, silt, or clay) that are used as the principal names of siliciclastic sediment. "Mud" refers to silt- and clay-sized particles (the graphic lithology pattern used is the one for "silty clay").
2. When two or more textural groups are present in a siliciclastic sediment in sufficient amounts, they are listed as principal names in order of increasing abundance.
3. The suffix "-stone" is affixed to the principal name sand, silt, and clay when the sediment is lithified (e.g., mudstone).

Lithologies consisting of >50% volcaniclastic components are referred to as "tephra."

Descriptive Terminology: Modifiers

The principal name of biogenic and siliciclastic sediments is preceded by major modifiers and followed by minor modifiers that may refer to mixed biogenic, siliciclastic, and volcaniclastic components:

1. 25%–50%: components in this range modify the principal name.
2. 10%–24%: components in this range are added with the suffix "-bearing" (e.g., foraminifer-bearing).
3. 0%–9%: components with these abundances are not named, unless they are very important for interpretation.

Descriptive Terminology: Examples

For a better understanding of the applied lithologic terminology, we give three examples:

1. An unconsolidated sediment containing 80% nannofossils, 13% silty clay, and 2% volcanic glass shards is termed "mud-bearing nannofossil ooze" (with minor volcanic glass shards).
2. A sediment containing 60% silty clay, 30% nannofossils, and 10% diatoms is termed "diatom-bearing nannofossil mud."
3. A friable sediment consisting of 50% nannofossils, 30% diatoms, and 20% foraminifers is referred to as a "foraminifer-bearing diatom nannofossil chalk."

Genetic Terminology

Visually distinctive glaciogenic sediment components are present in Leg 177 sediments, particularly ice-rafted debris (IRD). These sediments are described using the classification for siliciclastic sediments. They are often identified by the presence of isolated angular to subangular dropstones of varying composition and origin in the midst of fine-grained sediments as dropstone clusters, or as dropstones with other sand-sized IRD. Dropstones are defined as grains >1 cm in diameter. Characteristics of these sediments are detailed on core description forms within the general description portion of the lithologic description text.

In some core intervals, sediment composition and grain-size characteristics together with structural features (e.g., graded or contorted bedding) document sediment redeposition. In the barrel sheets, such lithologies are indicated by their descriptive terms with additional

remarks concerning their mode of transportation (e.g., "graded volcanic vitric ash layer that may represent a turbidite" or "contorted beds that probably originate from sediment slumping processes").

Visual Core Descriptions

The core description forms, or "barrel sheets" (Figs. F3, F4; see the "Core Descriptions" contents list), summarize the data obtained during a visual inspection of the core. The following text explains the ODP conventions used for compiling each part of the core description form and modifications to these procedures adopted by the Leg 177 scientific party.

Shipboard scientists were responsible for visual core inspection, smear-slide analyses, thin-section descriptions, and color analysis. Biostratigraphic (age), geochemical (calcium carbonate), and XRD (opal) data were integrated with other sedimentological information to augment core descriptions.

Cores are designated using leg, site, hole, core number, and core type information (see "Introduction," p. 1). The cored interval is specified in terms of mbsf and mcd (see "Composite Depths," p. 3).

Graphic Lithology

The lithology of the material recovered is represented on the core description form by up to three patterns in the column titled "Graphic Lithology" (Fig. F3). Constituents accounting for <10% of the sediment in a given lithology are not shown in the "Graphic Lithology" column and are not included in the lithologic name. The "Graphic Lithology" column shows only the composition of layers or intervals exceeding 20 cm in thickness.

Sedimentary Structures

In sediment cores, natural structures and structures created by the coring process can be difficult to distinguish. Natural structures observed are indicated in the "Structure" column of the core description form (Fig. F3). The symbols on the "Structure" column indicate the location of sediment features such as primary sedimentary structures, discrete trace fossils, soft-sediment deformation features, structural features, and diagenetic features. The apparent intensity of bioturbation is shown in the "Bioturbation" column of the barrel sheet in the conventional manner (none, rare, moderate, common, or abundant). Leg 177 sedimentologists recognize that sediment may be the product of deposition of material of homogeneous color and grain size resulting in sediment with no observable lamination or color change, or may be the product of total mixing by the action of bioturbating organisms. The symbols used to describe each of these biogenic and physical sedimentary structures are shown in Figure F4.

Sedimentary Disturbance

Deformation and disturbances of sediment that clearly resulted from the coring process are illustrated in the "Disturbance" column (Fig. F4). Blank regions indicate the absence of drilling disturbance. The degree of drilling disturbance is described for soft and firm sediments using the following categories:

F3. Example of a core description form (barrel sheet) used to describe sediment cores, p. 37.

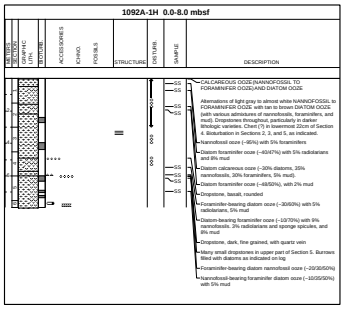

F4. Key to lithologic, disturbance, structure, fossil, and bioturbation symbols used in the core description forms, p. 38.

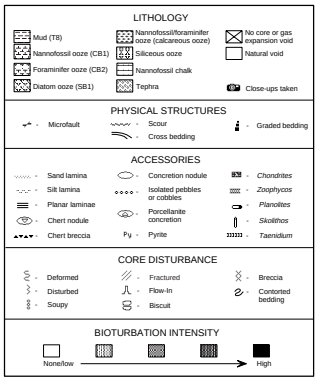

1. Slightly deformed: bedding contacts were slightly bent.
2. Moderately deformed: bedding contacts were extremely bowed.
3. Highly deformed: bedding was completely disturbed and in some places showed symmetrical diapir-like or flow structures.
4. Soupy: intervals were water saturated and had lost all aspects of original bedding.

The degree of fracturing in indurated sediments was described using the following categories:

1. Slightly fractured: core pieces were in place and contained little drilling slurry or breccia.
2. Moderately fragmented: core pieces were in place or partly displaced, but the original orientation was preserved or recognizable (drilling slurry may surround fragments).
3. Highly fragmented: pieces were from the cored interval and probably in the correct stratigraphic sequence (although they may not represent the entire section), but the original orientation was completely lost.
4. Drilling breccia: core pieces have lost their original orientation and stratigraphic position and may have been mixed with drilling slurry.

Samples

The positions of smear-slide samples taken from each core for shipboard analysis are indicated by "SS" in the "Sample" column on the core description form.

Tables summarizing data from smear-slide analyses appear in the "Core Descriptions" contents list. These tables include information on the sample location and core depth interval, whether the sample represents a primary or a minor lithology in the core, and the estimated percentages of identified components. The visual estimates are based on area percentage and are qualitative in nature.

Lithologic Description Text

The text describing the lithology, found in the "Description" column of the core description form, consists of two parts: (1) a heading that lists all the major sediment lithologies observed in the core, and (2) a general description of major and minor lithologies, including location of significant features in the core. Descriptions and locations of dropstones; concretions; thin, interbedded lithologies; and other minor lithologies are included in the text as is any clarifying information regarding sediment disturbance produced by drilling/coring or natural processes.

Color and Diffuse Spectral Reflectance

Qualitative visual impressions of sediment color were noted by sedimentologists as part of the core description process. In addition, quantitative estimates of sediment reflectance were collected using the Oregon State University Split Core Analysis Track (OSU-SCAT), an automated spectrophotometer, and the handheld Minolta CM-2002 spectrophotometer (see "Physical Properties," p. 21). As an aid to defining lithostratigraphic units, we employed the red band that is near the

instrument's maximum response. For shipboard analysis, the raw OSU-SCAT data were converted to percent reflectance and averaged into four 100-nm-wide bands defined as: (1) ultraviolet (UV; 250–350 nm), (2) blue (450–550 nm), (3) red (650–750 nm), and (4) near infrared (nIr; 850–950 nm). These bands are 50 nm wider than those used during previous ODP legs to allow integration of a greater fraction of the spectral signal. These bands were also used as an aid in constructing composite sections (see "Composite Depths," p. 3). The blue band is used for comparison to shipboard measurements of the calcium carbonate content of sediments because calcite has a somewhat higher reflectance at this wavelength than at longer wavelengths (see Mix et al., 1992).

X-ray Diffraction Measurements

Selected core samples were analyzed with an X-ray diffractometer (Philips PW 1729) to estimate opal contents and the composition of the terrigenous sedimentary fraction. Before XRD measurements, bulk-sediment samples were treated with 10% hydrochloric acid to remove the carbonate fraction, were washed for salt removal, oven dried at 105°C, and ground. This procedure may alter some clay mineral species but permits a quick shipboard XRD analysis within 1.5 days. Step scan measurements were run on random powder mounts with $Cu_{\kappa\alpha}$ radiation (40 kV and 35 mA) from 3° to 50°2θ at steps of 0.02°2θ per 2 s.

Graphic evaluation of the diffractograms was facilitated with the interactive MacDiff software (R. Petschick, public domain). It was used for mineral identification, on the basis of peak positions and relative intensities, as well as semiquantitative estimation of mineral abundances according to both peak intensities and integrated peak areas.

Opal contents were estimated from the maximum peak height of the broad opal hump at 24.5°2θ extending between 15° and 35°2θ in the X-ray diffractograms (Eisma and Van der Gaast, 1971; Hempel and Bohrmann, 1990). Eight external standard samples containing opal amounts between 5 and 70 wt% were run for calibration (Fig. F5). Opal standards consist of mixtures of pure diatom ooze, taken from a surface sample of the Conrad Rise in the western Indian Ocean sector of the Southern Ocean, and pure terrigenous sediment from the <63-µm fraction of a Quaternary till from the Baltic Sea, which shows a similar composition to terrigenous matter found in the Southern Ocean. Generally, a linear correlation exists between absolute intensities of the XRD opal hump of the standard samples and weight percentages of opal in the standard samples. Values of the regression equation depend on the XRD device, type of radiation, and the scan modes applied. For samples containing >10% opal, accuracy and precision of determined opal values are within ±3% of measured opal concentrations. Errors are higher for samples containing <10% opal.

Relative abundances of the minerals in the lithogenic fraction are presented only as relative changes in the peak areas or peak-area ratios of minerals. Diagnostic peaks of minerals found in the recovered sediments are (1) quartz (4.26 Å, multiplied by a factor of five for quantification), (2) feldspar (3.18–3.24 Å), (3) pyrite (2.71 Å), (4) clinoptilolite (8.9 and 7.9 Å), (5) hornblende (8.6 Å), and (6) clinopyroxene (3.0 Å). Clay mineral proportions were estimated collectively and are not clearly distinguished as individual clay mineral species. In X-ray diffractograms of random powder mounts, most clay minerals yield a broad diffraction peak at ~4.5 Å. The integral peak area can be used for the

F5. Linear regression between opal weight percentages and XRD counts, p. 39.

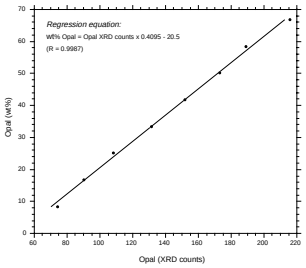

determination of clay mineral proportions. In some samples, a distinction between relative abundances of the 10-Å clay minerals (illite and sericite) and 7-Å clay minerals (kaolinite and chlorite) can be made using the 10-Å/7-Å peak intensity ratio. Smectite and mixed-layer clay minerals produce a very broad peak between 10 and 15 Å that is difficult to match precisely in the X-ray diffractograms.

XRD data are compiled in a separate table in the "Lithostratigraphy" section of each site chapter. We use the abbreviations Qz for quartz, Fsp for feldspar, and CM for clay minerals.

BIOSTRATIGRAPHY

Introduction

ODP Legs 113, 114, 119, and 120 resulted in an enormous improvement of southern high-latitude biostratigraphy. Cenozoic sequences recovered during these legs allowed the establishment of biostratigraphic zonations using calcareous and siliceous microfossils, and the resolution of species stratigraphic ranges that could be tied directly to the geomagnetic polarity time scale (GPTS) (e.g., Gersonde at al., 1990; Thomas et al., 1990; Barron et al., 1991; Harwood et al., 1992). Drilling during Leg 177 of a north-south transect will allow further improvement and refinement of these biostratigraphic schemes and the intercalibration of high- and mid-latitude zonations and species ranges. Improved dating of Neogene biostratigraphic ranges can be accomplished by correlation with orbitally tuned isotopic signals or other data sets with high temporal resolution, such as color reflectance, magnetic susceptibility, and paleointensity records. In addition, the transect of sites across the Southern Ocean provides a unique opportunity for documenting and understanding evolutionary processes (patterns, modes, and timing of speciation and diversification), the development of southern hemisphere bioprovinces (e.g., endemisms), and the response of the biota to long- and short-term environmental changes related to paleogeographic and cryospheric evolution in southern high latitudes.

Calcareous nannofossils, planktic and benthic foraminifers, diatoms, and radiolarians were examined for biostratigraphic zonation. The presence of other siliceous groups was routinely investigated (silicoflagellates, chrysophycean cysts, opal phytoliths, sponge spicules, ebridians, and the dinoflagellate *Actiniscus*). Depths (mbsf and mcd) given in the text for CC samples refer to the top of the sample interval.

Preliminary ages were assigned primarily by analysis of CC samples. Samples from within the cores were examined when a refined age determination was necessary. Correlations to standard chronostratigraphic frameworks will be determined postcruise by magnetobiostratigraphic studies and oxygen isotopic stratigraphy.

Ages for calcareous nannofossil, foraminifer, diatom, and radiolarian datum events, and epoch boundaries are based on the GPTS of Berggren et al. (1995a, 1995b) (Fig. F6).

Micropaleontological data, including total and species abundance and preservation, are summarized in separate tables in the "Biostratigraphy" section of each site chapter.

F6. Biostratigraphic zonal schemes tied to the geomagnetic polarity time scale, and age assignments, p. 40.

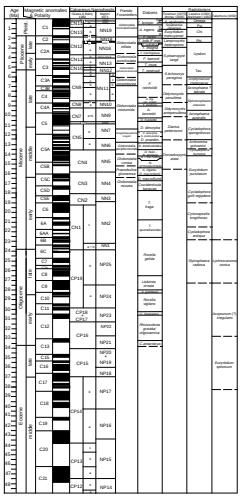

Calcareous Nannofossils

During Leg 177, we employed the zonal schemes of Martini (1971) and Bukry (1973, 1975) with code numbering by Okada and Bukry (1980). These zonations are regarded as the standard framework for the biostratigraphic subdivision of low-latitude Cenozoic marine sediments based on calcareous nannofossils, and some of these events are also identifiable in middle to high latitudes. In addition to the classical concept of first/last occurrences of index species, we used ranges of taxa to improve the stratigraphic resolution of the Pleistocene interval. This includes the commonly used *Emiliania huxleyi* acme zone that roughly spans the last 90 k.y. (Thierstein et al., 1977), and the "Small *Gephyrocapsa* Zone" of Gartner (1977), an interval that defines the last 300 k.y. of Okada and Bukry's CN13b biozone. According to the Leg 175 Shipboard Scientific Party (1998b), this interval ranges from marine isotopic Stage (MIS) 30 to 44. The top of the *Gephyrocapsa caribbeanica* acme Zone, dated at 260 ka, is approximately synchronous with the first occurrence (FO) of *E. huxleyi* (Pujos, 1988), and thus provides a useful alternative to identify the base of Martini's NN21 Zone. Likewise, ages of most calcareous nannofossil data employed to construct the Leg 177 age model for the Pliocene–Pleistocene interval come from the work of Raffi et al. (1993) and Wei (1993). For the Miocene–Eocene interval we follow the biochronology proposed by Berggren et al. (1995b) as well as other authors referenced in Table **T1.** Where datums used by Martini (1971) and Okada and Bukry (1980) were not identifiable, additional data were used from the Paleogene–lower Neogene zonal schemes of Wise (1983), Wei and Wise (1990), and Crux (1991) (Table **T1;** Figs. **F6**, **F7**).

T1. Calcareous nannofossil datums used during Leg 177 and their assigned age estimates, **p. 49.**

F7. Geomagnetic polarity time scale, biostratigraphic zonations, and selected datums used, **p. 41.**

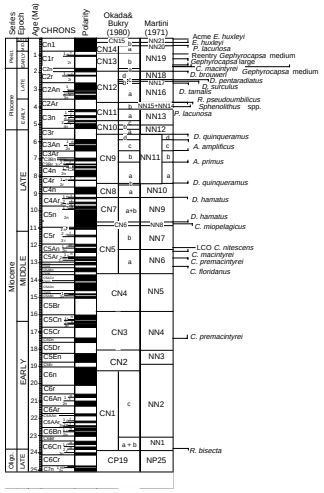

Relative abundance of nannofossils was described by five categories:

D = dominant, >50% of the total assemblage;
A = abundant, 10%–50% of the total assemblage;
C = common, 1%–10% of the total assemblage;
F = few, 0.1%–1% of the total assemblage; and
R = rare, <0.1% of the total assemblage.

Total abundance of calcareous nannofossil for each sample was estimated as follows:

VA= very abundant, >100 nannoliths per field of view;
A = abundant, 10–100 nannoliths per field of view;
C = common, 1–10 nannoliths per field of view;
R = rare, < 1 nannolith for 10 fields of view; and
B = barren.

Planktic Foraminifers

Several zonal schemes have been developed for the mid- and high-latitudes of the Southern Hemisphere (e.g., Jenkins and Srinivasan, 1986; Berggren, 1992a; Berggren et al., 1995b). On the basis of previous work (Brunner, 1991; Pujol and Bourroiulh, 1991), the late Neogene subantarctic zonation scheme of Jenkins and Srinivasan (1986) (Table T2) was selected to biostratigraphically subdivide the sequences recovered during Leg 177 (Fig. F6). However, this zonation scheme was not fully applicable to the foraminifer fauna in all sediments because of the absence or low abundance of several marker species.

T2. Planktic foraminifer Subantarctic zonal scheme (Jenkins and Srinivasan, 1986), p. 51.

Methods

Sediment samples were soaked in tap water and then washed over a 63-µm sieve. The sieves were soaked in water containing Methylene Blue between successive samples to stain specimens left in the sieve from previous samples. All samples were dried under heat lamps.

Planktic foraminifer species abundances (as percentages of the total assemblage) were defined as follows:

D = dominant, >30%;
A = abundant, 10%–30%;
F = few/frequent, 5%–10%;
R = rare, 1%–5%;
P = present, less than 1%; and
B = barren.

Preservation was categorized as follows:

G = good (dissolution effects are rare);
M = moderate (dissolution damage, such as etched and partially broken tests, occurs frequently and fragments are abundant); and
P = poor (the degree of fragmentation is often high and the specimens are often small, compact, and encrusted).

The abundance of planktic foraminifers as a group relative to the total residue was categorized as follows:

A = abundant, >50%;
C = common, 25%–50%;
F = few, 10%–25%;
R = rare, less than 5% of the residue;
T = trace, trace was used in the case where only a few broken tests were recorded in a sample; and
B = barren, no specimens in sample.

The generic classification used mainly follows that of Kennett and Srinivasan (1983). However, the taxonomy of *Globorotalia* follows Scott et al. (1990). Species identification of Paleogene and early Neogene planktic foraminifers follows Stott and Kennett (1990) and Berggren (1992b).

Benthic Foraminifers and *Bolboforma*

Benthic foraminifers provide limited biostratigraphic age control for Leg 177 samples, and all zones recognized are local assemblage zones. Individual benthic foraminifer datums are recognized and discussed for each site. Particularly useful, but requiring further study, is the last occurrence (LO) of *Stilostomella lepidula* at about 0.9 Ma. Additional age-diagnostic taxa include the LO of *Alabamina dissonata* at Site 1090 which marks the latest Eocene, the LO of *Nuttallides truempyi* which is considered by Berggren and Aubert (1983) to provide a useful marker of the Eocene/Oligocene boundary, or the presence of *Aragonia aragonensis* which provides a potentially valuable indication of latest middle Eocene age.

Taxonomic assignments follow those of van Morkhoven et al. (1986), Thomas (1990), and Mackensen (1992).

Bolboforma were recovered from Site 1092 and taxonomic concepts are based on Qvale and Spiegler (1989) and Spiegler (1991). Stratigraphic subdivision is largely based upon Norwegian Sea material and is therefore of limited value for a detailed stratigraphic subdivision of the middle to late Miocene at Site 1092. However, the work of Spiegler (1991) on Leg 114 material from the South Atlantic Ocean and Mackensen and Spiegler (1992) on Leg 120 material from the Kerguelen Plateau in the southern Indian Ocean, suggests that there is some potential to improve the biostratigraphic utility of this group in the Southern Ocean.

Methods

To obtain planktic and benthic foraminifers and *Bolboforma* from CC samples, a 20-cm^3 sample was disaggregated and washed over a 63-µm sieve. At the southernmost sites, highly abundant, needle-shaped remains of the diatom genus *Thalassiothrix* in the >63-µm fraction made it necessary to wet-sieve sediment samples at 150 µm. Cursory examination of the 63- to 150-µm fraction reveals that significant components of the benthic assemblage are retained within this size range, notably phytodetrital taxa such as *Alabaminella weddellensis* and *Epistominella exigua*. Between samples, sieves were soaked in a solution of Methylene Blue to stain foraminifers and identify potential contamination. The samples were dried under heat lamps and benthic foraminifers were examined from the entire >63- or >150-µm fraction under the binocular microscope and identified, where possible, to species level. Species abundances were determined from numeric population counts

that typically ranged from 100 to 300 specimens per sample. The relationship between number of specimens and number of taxa observed in all Leg 177 samples is summarized in Figure F8. The figure clearly illustrates that counts of >250–300 specimens are required to obtain reliable estimates of species richness and diversity; it should be noted, however, that many of the 20-cm³ samples yielded only low foraminifer numbers. Quantitative estimates of foraminifer abundance were made at each site by multiplying foraminifer sums by the fraction of the coarse residue studied. Where time did not allow for large counts, species abundances were recorded as follows:

D = dominant, >50% of total assemblage;
A = abundant, 10%–50% of total assemblage;
C = common, 1%–10% of total assemblage;
F = few, 0.1%–1% of total assemblage;
R = rare, <0.1% of total assemblage; and
B = barren, no specimens observed.

Preservation was categorized as G (good), M (moderate), or P (poor).

Diatoms

Diatom biostratigraphic studies made during Leg 177 follow the zonal schemes developed for the southern high latitudes by Gersonde and Burckle (1990), Baldauf and Barron (1991), Harwood and Mayurama (1992), and Gersonde and Bárcena (1998), as combined by Gersonde et al. (1998). Two biostratigraphic zones have been preliminarily revised. The FO of *Thalassiosira vulnifica,* which marks the base of the *Thalassiosira insigna–T. vulnifica* Zone of Harwood and Maruyama (1992), is probably diachronous, and we replaced this zone by one tentatively named the *T. insigna* Zone. The bottom and top of this zone are defined by the FO and LO of the nominate taxon, respectively. On the basis of preliminary biostratigraphic age assignments, the basal age of the *Fragilariopsis reinholdii* Zone, marked by the FO of the nominate taxon, was placed in Chron C4 at ~8.1 Ma, an age that is close to the age of its FO in the equatorial Pacific Ocean, as reported by Barron (1992).

Because of the presence of warm and temperate species in the northernmost sites of Leg 177, additional stratigraphic ranges have been added following the compilation of Barron (1992). This zonation and the individual species ranges cover a time interval spanning the early Oligocene to Pleistocene and are tied to the GPTS of Berggren et al. (1995a, 1995b) as presented in Figures F6 and F9.

Age assignments of the zones and species ranges employed are compiled in Tables T3 and T4. For stratigraphic age assignment of Paleogene sections we combined diatom zones and species ranges published by Gombos (1983), Gombos and Ciesielski (1983), and Fenner (1984). These are not yet tied to the GPTS.

The diatom assemblages observed in sediments recovered during Leg 177 also provide paleoenvironmental information, such as the thermal isolation of the Southern Ocean, changes in the late Quaternary surface-water temperatures, and Antarctic sea-ice extent. The presence of freshwater and benthic marine diatoms at Leg 177 sites indicates advection by eolian and/or lateral transport.

F8. Number of benthic foraminifer species identified vs. number of specimens counted, p. 43.

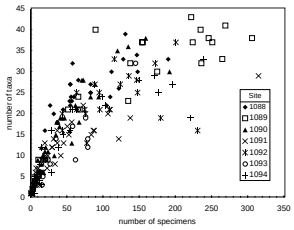

F9. Diatom zonation and stratigraphic ranges of diatom species, p. 44.

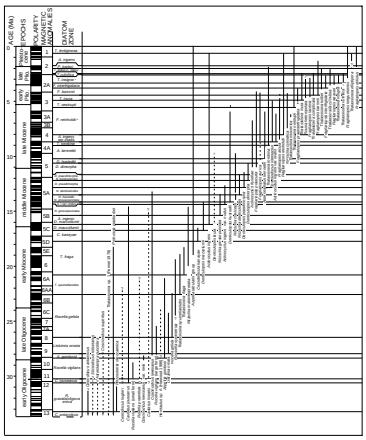

T3. Age assignments of biostratigraphic diatom zones used during Leg 177, p. 52.

T4. Compilation of diatom species ranges, p. 53.

Methods

Two type of slides were prepared for diatom analysis, depending on overall diatom abundance. For intervals rich in biogenic silica (e.g., sites in the circum-Antarctic opal belt; see "Leg 177 Summary" chapter), smear slides were prepared from a small amount of raw material in a CC or from additional core material when required. In intervals dominated by carbonate and poor in silica, a small amount of sample was immersed in 10% HCl to remove calcium carbonate. The carbonate-free residue was repeatedly washed with distilled water to remove the acid. In each case, aliquots of raw and cleaned sample were mounted as a thin film on microslides, protected by 18-mm-diameter cover glass slips using Mountex mounting medium. All slides were examined in their entirety with a Zeiss compound microscope at a magnification of 400× for stratigraphic markers and paleoenvironmentally sensitive taxa. Species identification was confirmed when necessary at 1000×. The counting convention of Schrader and Gersonde (1978) was adopted. For documentation of poorly known or undescribed taxa, photomicrographs were made using a video-print system at 1500× final magnification.

Overall diatom abundance was determined based on smear-slide evaluation at 400×, using the following convention:

A = abundant, >300 valves per traverse of microslide (>10 per field of view);
C = common, 100–300 valves per traverse of microslide (3–10 per field of view);
F = few, 30–100 valves per traverse of microslide (1–3 per field of view);
R = rare, 5–30 valves per traverse of microslide;
T = trace, <5 valves per traverse of microslide; and
B = barren, no diatoms in sample.

The species relative abundance was defined as follows:

D = dominant, >60% of assemblage;
A = abundant, 30%–60% of assemblage;
C = common, 15%–30% of assemblage;
F = few, 3%–15% of assemblage;
R = rare, <3% of assemblage;
T = trace, sporadic occurrence; and
X = present, presence was indicated in cases where diatom valves could not be counted individually (e.g., *Ethmodicus rex* fragments) or for all taxa encountered in samples with trace/rare overall abundance.

Preservation of diatoms was determined qualitatively as follows:

G = good (lightly silicified forms present and no alteration of frustules observed);
M = moderate (lightly silicified forms present, but with some alteration); and
P = poor (finely silicified forms absent or rare and fragmented, and the assemblage is dominated by robust forms).

At several sites, preservation and abundance estimates were plotted vs. depth to visualize the distribution of diatom abundance and preservation. For computing purposes, a number was assigned to each overall diatom abundance category: abundant = 18, common = 9, few = 3, rare = 1, trace = 0.5, and barren = 0. To show individual species or species group abundance we assigned the following numbers: dominant = 100, abundant = 60, common = 30, few = 15, rare = 3, trace = 0.5, and barren = 0. Assemblage preservation categories were designated as good = 3, moderate = 2, or poor = 1.

Radiolarians

Neogene to Paleogene radiolarian zones used in this study mainly follow those of Abelmann (1992), Lazarus (1992), and Takemura (1992). However, radiolarian assemblages from the northern sites of the Leg 177 transect include low- to mid-latitude zonal markers, which prevent application of the Antarctic/Subantarctic zonal scheme. In such cases, a tentative age assignment was made using the mid-latitude zonation of Foreman (1975) and Morley (1985), established in the North Pacific region. Applicability of the Indian and Pacific low-latitude zonations (Johnson et al., 1989; Moore, 1995) is not yet confirmed. Figure F6 and Table T5 show the radiolarian zonations and datums, respectively, used during Leg 177. Precise correlation between the Antarctic and mid-latitude zonations remains preliminary. It is expected that additional radiolarian datums will be identified by shore-based biostratigraphic studies.

T5. Ages of biostratigraphically useful radiolarian datums calibrated to the Berggren et al. (1995b) geomagnetic polarity time scale, p. 55.

Methods

To obtain radiolarians from CC samples, ~10 cm^3 of sediment was disaggregated and boiled with 10% H_2O_2, 10% HCl, and ~1% Calgon solutions. Brief treatment of samples in an ultrasonic bath was followed by washing on a 63-µm sieve. The residue was transferred to a beaker, and a strewn slide was made using a pipette. Canada Balsam was used as a mounting medium. Additional random strewn slides will be prepared on shore to locate biostratigraphic events more accurately within cores.

Overall radiolarian abundance was determined by strewn slide evaluation at 100×, using the following conventions:

A = abundant, >100 specimens per slide traverse;
C = common, 50–100 specimens per slide traverse;
F = few, 10–50 specimens per slide traverse;
R = rare, <10 specimens per slide traverse; and
B = barren, no radiolarians in sample.

The abundance of individual species was recorded relative to the fraction of the total assemblage as follows:

A = abundant, >10% of the total assemblage;
C = common, 5%–10% of the total assemblage;
F = few, <5% of the total assemblage;
R = rare, a single to few specimens per slide; and
B = barren, absent.

Preservation was recorded as follows:

E = excellent (nearly pristine, complete skeleton, lacking any indication of dissolution, recrystallization or breakage);
G = good (majority of specimens complete; minor dissolution, recrystallization and/or breakage);
M = moderate (minor but common dissolution, small amount of recrystallization or breakage of specimens); and
P = poor (strong dissolution, recrystallization or breakage, many specimens unidentifiable).

PALEOMAGNETISM

Paleomagnetic studies conducted during Leg 177 comprised long-core magnetic remanence measurements of archive-half sections before and after alternating-field (AF) demagnetization. In addition, a small number of magnetic remanence measurements were made on discrete samples collected from the working halves of cores.

Long-core remanence measurements and AF demagnetizations were performed using a long-core cryogenic magnetometer (2G Model 760-R) with an in-line AF demagnetizer capable of reaching peak fields of 80 mT. Archive halves were measured for all core sections not disturbed by drilling. The number of demagnetization steps applied to each core section was controlled by time constraints and core flow through the laboratory, rather than magnetic properties of the cores themselves. A six-step demagnetization scheme (taking about 20 min) was applied to most 1.5-m-long core sections. This standard measurement scheme involved stepwise demagnetization at 0 (natural remanent magnetization), 5, 10, 15, 20, and 25 mT. At Hole 1090C, a three measurement scheme (0, 10, and 20 mT) was applied to increase core flow through the laboratory. At all other holes, either a four-, five-, or six-step measurement scheme was used. At Site 1091, archive halves were demagnetized at peak fields of 30 mT. At all other sites, the peak demagnetizing fields were 20 or 25 mT. The low peak demagnetization fields ensure that the archive halves remain useful for shore-based high-resolution (U-channel) magnetic studies. We used a 5-cm sample interval for long-core remanence measurements, starting 20 cm above the core-section top and ending 20 cm below the core-section base. The large leader and trailer distance (20 cm) was used to allow future deconvolution of the long-core data. For shipboard analysis, we disregarded measurements within 10 cm from the ends of each section.

Discrete samples were collected from working halves in standard (6 cm^3) plastic cubes, with the arrow on the sampling box pointing upcore. The sampling frequency was generally one sample per core section at one hole per site. Intervals of drilling-related core deformation were avoided. The discrete samples will be analyzed on shore to (1) ground-truth the shipboard polarity stratigraphies, and (2) gain insight into the magnetic properties of the sediments and the mineralogy of the remanence carriers. The shipboard long-core magnetometer was used to measure the remanence of a small number of discrete samples, using a measurement tray designed for six samples.

Where magnetic cleaning successfully isolated the primary (characteristic) component of remanence, paleomagnetic inclinations were used to define polarity zones. All cores were, to a greater or lesser extent, affected by a steep downward viscous remanent magnetization attributed to the drill string. At most Leg 177 sites, this secondary magnetization could be removed by peak demagnetization fields in the 10-

to 15-mT range. However, higher coercivity secondary magnetizations, tentatively attributed to the effects of reduction diagenesis particularly at Sites 1091 and 1093, were more difficult to remove and were not always removed at the peak demagnetization fields utilized on board (25 or 30 mT). The revised time scale of Cande and Kent (1995) was used as a reference for the ages of Cenozoic polarity chrons.

Tensor core orientation data were available for Holes 1088B, 1088C, 1089A, 1089B, 1089C, 1090D, 1090E, 1091A, 1091B, 1093A, 1093B, 1093C, and 1094A. At the other holes, the Tensor tool was not employed because of bad weather conditions or time constraints. At Site 1093, one of the two Tensor tools malfunctioned resulting in sporadic orientation data. At Hole 1094A, repeated failure of the Tensor tool resulted in one out of every five cores being oriented.

The magnetic susceptibility was measured for each whole-core section as part of the MST analysis. The MST susceptibility meter (a Bartington MS2C meter with an 88-mm coil diameter and a 0.565-kHz frequency) was set on SI units and the output values were stored in the JANUS database. To convert the database values into SI units of volume magnetic susceptibility, they should be multiplied by 10^{-5} and by a correction factor that takes into account the volume of material that passed through the susceptibility coils. Except for measurements near the ends of each section, this factor for a standard ODP core is ~0.63 (see also **"Physical Properties,"** p. 21; Blum, 1997). We confirmed that this correction factor was appropriate by comparing the MST magnetic susceptibility data from ODP Leg 162 with U-channel data from the same cores. The U-channel susceptibility data were measured at Gif-sur-Yvette (France) on a susceptibility track that has been carefully calibrated.

GEOCHEMISTRY

Interstitial Water Sampling and Chemistry

Shipboard interstitial water analyses were performed on 5- to 10-cm whole-round sections cut immediately after the core was sectioned on deck. At Holes 1088B and 1093A, relatively closely spaced samples were taken for interstitial water analyses from the bottom of each section (except the last section) for the first 60 mbsf, one sample per core was taken to ~100 mbsf, and then one sample every other core to depth. At other sites, samples were usually taken from the fourth section from the top of each core, away from any possible drilling disturbance (see site chapters for details).

Interstitial water samples were collected with titanium squeezers that are modified versions of the standard ODP stainless steel squeezer of Manheim and Sayles (1974). Each whole round was carefully scraped free of the outer rind with a stainless steel spatula, then squeezed through one or two Whatman No. 1 filters prerinsed in high-purity water, and then through a 0.45-µm Gelman polysulfone disposable filter into a 50-mL plastic syringe. Interstitial waters were extruded by applying pressures up to 40,000 lb using a Carver Laboratory Press (Model 2702). After collection of 40 to 50 mL of interstitial water, the syringe was removed, a fresh 0.45-µm Gelman filter was attached, and aliquots were dispensed into plastic vials for shipboard analyses and into acid-washed plastic vials and 5-mL glass ampoules (flame sealed) for future shore-based work.

Interstitial waters were routinely analyzed for salinity, as total dissolved solids, with a Goldberg optical handheld refractometer (Reichart). Alkalinity and pH were measured immediately after squeezing by Gran titration with a Metrohm autotitrator and a Brinkmann pH electrode, respectively. Chloride was measured by titration with $AgNO_3$.

Na, K, Mg, Ca, Cl, and SO_4 were measured by ion chromatography on 1:200 diluted aliquots in nanopure water using a Dionex DX-100. In general, the results obtained for some elements from this technique are less accurate than alternate methods, including titration for Cl and charge balance calculations for Na. However, the relative trends are usually similar and can serve as a second check of the results generated by other methods. The precision of results measured by ion chromatography was generally within 3%–5%. The Cl and Na measurements obtained by ion chromatography are not reported here.

Silica, ammonia, and phosphate were determined by colorimetic methods using a Milton Roy Spectronic spectrophotometer with a 1-cm cell and sample introduction by Mister Sipper. The chemical methods employed follow those of Gieskes et al. (1991). Sodium was estimated by charge balance where total cation charge equals total anion charge. For most of these analyses, the International Association of Physical Sciences Organizations (IAPSO) seawater standard was used for standardization.

Strontium, lithium, iron, and manganese were determined using a Varian Spectra AA-20 atomic absorption spectrophotometer. Samples for iron and manganese were acidified with 50 µL triple-distilled HCl per 5 mL immediately after collection. Standards were matched in matrix composition to the samples. Lithium and manganese standards and samples were determined on 1:5 diluted aliquots in nanopure water and 0.1 N HCl, respectively. Strontium was determined on 1:10 diluted aliquots, and iron was determined without dilution. Lithium was determined by emission using an air-acetylene flame. Strontium, manganese, and iron were determined by atomic absorption using an air-acetylene flame. Strontium and manganese utilized lanthanum chloride as an ionization suppressant. The precision of these techniques is approximately <1%–2% for lithium and <4% for strontium, manganese, and iron.

The iron measurements should be interpreted with caution primarily for two reasons: (1) it was not possible to squeeze sediment samples under oxygen-free conditions and still maintain timely processing of interstitial waters through the chemistry laboratory; thus, some dissolved Fe^{+2} may have oxidized, been trapped on filters, or been lost to the walls of the syringe; and (2) some colloidal iron oxides are able to pass through 0.45-µM filters. The first effect would cause Fe^{+2} concentrations to be underestimated, whereas the second could result in an overestimation. Despite these potential problems, the iron data reported here are probably at least qualitative representations of the true in situ iron concentrations.

Organic Geochemistry

The shipboard organic geochemistry program for Leg 177 included the following: (1) real-time monitoring of volatile hydrocarbon gases; (2) measurement of the inorganic carbon concentrations to determine the amount of carbonate in the sediments; (3) elemental analyses of total carbon, total nitrogen, and total sulfur; and (4) preliminary characterization of organic matter. All methods and instruments used dur-

ing Leg 177 are described below. Additional details are available in Emeis and Kvenvolden (1986). These analyses were conducted as part of the routine shipboard safety requirements, and to provide information for preliminary site summaries and shore-based organic geochemical research.

Hydrocarbon Gases

For safety considerations, the concentrations of methane (C_1), ethane (C_2), and propane (C_3) gases in the sediments were measured at frequencies of generally one per core. The headspace method was used throughout the cruise. Gases released by the sediment after core recovery were analyzed by gas chromatography (GC) using the following technique. Immediately after retrieval on deck, a calibrated cork borer was used to obtain a measured volume of sediment from the top of one section for each core. The sediment, with a typical volume of ~5 cm^3, was placed in a 21.5-cm^3 glass serum vial that was sealed with a septum and metal crimp cap. When consolidated or lithified samples were encountered, chips of material were placed in the vial and sealed. Before gas analysis, the vial was heated to 60°C for 30 min. A 5-cm^3 volume of the headspace gas was extracted from each vial using a standard glass syringe. Vacutainer samples were not taken during this leg because gas voids were not present in the core. The collected gas was analyzed by a gas chromatograph (Hewlett Packard 5890 II Plus) equipped with a 60 m × 0.32 mm DB-1 capillary column and a frame ionization detector. Helium was used as a carrier gas and a Hewlett Packard Chemstation was used for data acquisition and processing. Chromatographic response was calibrated against pre-analyzed standards; gas contents are reported in parts per million by volume.

Inorganic Carbon

Inorganic carbon is determined using a Coulometric 5011 carbon dioxide coulometer. A sample of ~10 mg of freeze-dried, ground sediment was reacted with 2N HCl. The liberated CO_2 was back-titrated to a colorimetric end point. The percentage of carbonate is calculated from the inorganic carbon (IC) content with the assumption that all inorganic carbon is present as calcium carbonate:

$$\%CaCO_3 = \%IC \times 8.33. \quad (1)$$

Elemental Analyses

The total carbon (TC), total nitrogen (TN), and total sulfur contents of the sediment are determined using a Carlo Erba Model NA1500 carbon-nitrogen-sulfur analyzer. A sample of ~6 mg of freeze-dried, ground sediment was combusted at 1000°C in a stream of oxygen. Helium was used as a carrier gas, the oxygen was removed, and the combustion products were reduced. The reduced gases were separated by GC and quantified with a thermal conductivity detector. Contents of total organic carbon (TOC) were calculated as the difference between TC and IC:

$$TOC = TC - IC. \quad (2)$$

The origin of the organic matter in the sediments can be characterized using organic carbon/nitrogen (C/N) ratios. Organic matter atomic C/N ratios were calculated from the TOC and TN concentrations. The average C/N ratio of marine zoo- and phytoplankton is between 5 and 8, whereas fresh higher land plants have ratios between 25 and 35 (e.g., Emerson and Hedges, 1988; Meyers, 1994). Pyrolysis analyses were not performed because TOC contents were generally low in the Leg 177 sediments.

PHYSICAL PROPERTIES

Introduction

The purpose of physical properties measurements conducted during Leg 177 was to provide (1) near-continuous records for hole-to-hole correlation, the construction of complete stratigraphic sequences, and core-to-downhole log ties; and (2) estimates of properties related to composition of the sediments, which can then be used as high-resolution proxy records related to paleoenvironmental changes.

The first measurement station was the MST, which combines four sensors on an automated track to measure bulk density, magnetic susceptibility, natural gamma-ray emission, and *P*-wave velocity on whole-core sections. Next, thermal conductivity was measured on whole-core sections in intervals where downhole temperature measurements were taken. Then, the cores were split and the working half was used for further physical properties measurements. These included diffuse spectral reflectance and resistivity measured with the OSU-SCAT, *P*-wave velocity, water content, and grain density measurements to calculate bulk density, porosity, and related properties. Most of the methods are described in detail in the Physical Properties Handbook (Blum, 1997) and are summarized here.

Bulk Density (Gamma-ray Attenuation)

Estimates of bulk density were obtained from MST GRA measurements of whole-round core sections at intervals of 2 cm and 4 s sampling time. The calibration was based on aluminum standards of different thickness mounted in a water-filled core liner (Blum, 1997). This calibration takes into account (1) the higher Compton attentuation coefficient in water compared to common minerals, (2) count rate effects (Weber et al., 1997), and (3) a correction for the core liner. For each site, we calculated the correlation between the GRA bulk densities and the bulk densities determined on core specimens using the moisture-density method (see below). GRA densities were ~5% higher than bulk densities measured on discrete samples. This discrepancy will be investigated postcruise by grain-density measurements on dry samples.

Natural Gamma-ray Emission

Natural gamma-ray measurements were taken for periods of 4 s every 2, 4, or 8 cm, depending on time constraints determined by core flow through the laboratory. Calibration was performed at the beginning of the leg and at Site 1093. Background radiation was determined with a water core to be about 14 cps. No subtraction of background radiation

was done on the data presented in the plots. The total counts were useful for definition of some lithologic trends.

Although measuring time was 4 s, the MST program needed 6 additional seconds to upload the measured counts at each 2-cm step. During the upload time, the measurement systems were idle, slowing down the core flow. However, combined MST measurements made at 2-cm resolution and 4-s measuring time, still took no more than 21 min per core section in total. This did not exceed the standard run time (21 min/section) that it takes for a core to move through the cryogenic magnetometer. As a result of an electronic malfunction, data collected from Cores 177-1092B-14H through 177-1093C-5H showed a great degree of scattering. This was also seen in the control measurements after each section (Fig. F10).

F10. Control measurements of NGR emission at Sites 1092 and 1093, p. 45.

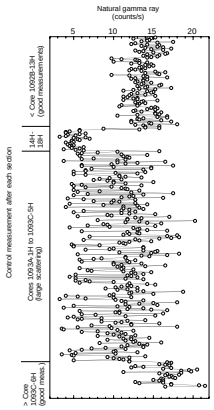

Magnetic Susceptibility

Magnetic susceptibility was measured with the Bartington meter MS2 using an 8-cm loop and the low sensitivity setting of 1.0 Hz. Sample periods were 4 s and sampling intervals 2 cm. The mean value of the four measurements was stored. Volume-normalized SI units ($\times 10^{-5}$) for the magnetic susceptibility were calculated from the sensor signals by multiplication with a factor of 0.63 (coil-to-core diameter ratio, Bartington manual; Shipboard Scientific Party, 1994). Magnetic susceptibility was one of the most useful records for core-to-core correlation and composite depth construction.

Thermal Conductivity

Thermal conductivity measurements are required for geothermal heat flow determinations. Thermal conductivity was measured after the cores had equilibrated to ambient temperature, about 3–4 hr after recovery, using a single-needle probe, in full-space configuration (von Herzen and Maxwell, 1959; Blum, 1997). Data are reported in W/(m·K) with an estimated error of ~5%.

Reference measurements of a red rubber standard, conducted while occupying Sites 1088, 1092, 1093, and 1094, gave a value of 0.870 ± 0.014 W/(m·K) (1.7% error; Table T6, also in ASCII format in the TABLES directory). This standard was particularly useful because the value is close to those obtained from the cores drilled during Leg 177. The empirical value for the red rubber standard, obtained during early ODP operation and used during recent legs, is 0.96 ± 0.05 W/(m·K). We suggest that the Leg 177 value obtained with the new TK04 unit (see Blum [1997] for description and references) is more accurate and precise.

T6. Control measurements of thermal conductivity in red rubber, p. 56.

Moisture and Density

Moisture and density (MAD) measurements, as defined for ODP shipboard procedures, include gravimetric determinations of water content, bulk density, grain (solid) density, and related properties such as porosity, void ratio, and dry density. Initial wet bulk mass (M_b), dry mass (M_d), and volume (V_d) were measured after drying the samples in a convection oven for 24 hr at temperatures of 105°C. Tests conducted at the beginning of Leg 177 with samples dried at 60° and 105°C, and freeze-drying with and without frozen samples showed that freeze-drying for 24 hr would give comparable results (Fig. F11). Freeze-dried samples

F11. Comparison between oven drying and freeze-drying of samples, p. 46.

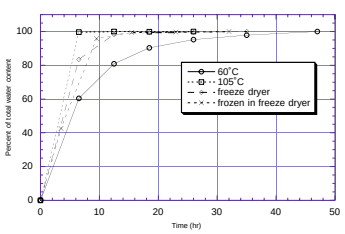

could still be used for further sedimentological investigations (clay mineralogy, grain size, etc.), whereas oven drying may alter the clay mineralogy and causes problems for the disaggregation of the samples.

Samples collected for MAD measurements were taken at an average frequency of one per core section. However, where frequent lithologic changes occurred, denser sampling was undertaken to ensure measurements were available from all significant lithologies throughout the core. In cores of particularly homogeneous lithology, the sampling interval was reduced to two samples per core. The MAD samples were taken at the same position as measurements of *P*-wave velocity (see below). This ensures that the different parameters represent the same sediment type, and can be correlated without interpolation. In XCB cores, which frequently showed "biscuiting" type of disturbance, particular care was taken to sample undisturbed parts of the core sections and to avoid the drilling slurry.

Velocity

P-wave velocity was measured orthogonal to the core axis in steps of 2–4 cm on whole-round core sections with the *P*-wave logger (PWL) mounted on the MST. At Sites 1088 through 1092, PWL data were compromised because of a malfunctioning calibration screw for setting threshold detection. This was finally repaired in Section 177-1093A-5H-1, and the detection delay was changed from 2 to 3 µs because the first excursion of the received signal was negative (Blum, 1997). Data collected before the repair can be salvaged after filtering and correction using the *P*-wave velocity sensor 3 (PWS3) measurements (see below).

In addition, *P*-wave velocity was measured on split-core sections using the PWS3 contact probe system (a modified Hamilton frame), which measures orthogonal to the core axis across the split-core section and core liner through transducer contact with the sediment on top and the core liner on bottom, respectively. Two types of *P*-wave transducer pairs (PWS1 and PWS2), inserted along and orthogonal to the core axis into soft sediment, were used in only a few intervals to minimize core disturbance. If a signal was retrieved, the *P*-wave velocity was comparable to the corresponding velocity obtained from the PWS3 probe.

The PWS1 split-core velocimeter calculates velocity based on a fixed distance and measured traveltime. In addition to traveltime, the PWS3 system measures variable sample thickness with a digital micrometer that is zeroed periodically. The calibration procedures for both the PWL and PWS3 were done after Blum (1997).

Reflectance

Quantitative estimates of sediment diffuse spectral reflectance and resistivity were generated by the shipboard sedimentologists using the OSU-SCAT. The handheld, Minolta CM-2002 spectrophotometer was also used to measure sediment color reflectance on selected intervals. The OSU-SCAT spectrophotometer system (Mix et al., 1992) consists of a computer-controlled motorized-track assembly that advances a core section into sampling position under a commercially available light integration sphere. The integration sphere is brought into contact with the sediment via a computer-controlled vertical stepping motor. Temperature, conductivity, and strain sensors detect contact with the sediment surface and provide measurements of sediment resistivity (see

"Resistivity," p. 25). During operation, light with known spectral characteristics passes through fiber optics and is steered using a directional mirror toward two reference ports and a measurement port. The light that is diffusely reflected off the sediments is integrated within the sphere, split into constituent wavelengths by a diffraction grating, and collected with a multichannel detector.

An earlier version of this instrument was employed during Leg 138 (Mix et al., 1992). The current version was used for postcruise analysis of cores collected during Leg 154, and for shipboard analysis of cores during Legs 162 and 167. The new design has incorporated four improvements: (1) the addition of the integration sphere; (2) the use of a motorized mirror for source-beam direction, rather than a source-beam splitter; (3) determination of internal "white" reference on each sample and "black" background estimations for all standards and alternating samples; and (4) the spectral range of the instrument was extended beyond the visible to include both UV and nIR wavelengths. These improvements have increased the signal-to-noise ratio considerably over the earlier version of the instrument.

Reflected light was measured in 1024 bands of 0.682-nm width ranging from 250 to 950 nm at Site 1088, but in the visible and nIR range only (~400–950 nm) at Sites 1089–1094 because of a failure of the UV light source. It would have been desirable to measure all core sections from all multiple holes at 2-cm intervals, comparable to MST measurements. However, time constraints and the relatively slow vertical motion of the integration sphere limited the measurement program to 4- to 6-cm intervals on all APC and some XCB cores from one designated hole at each site (usually the A hole), and on chosen intervals from the other holes at each site. As a result of this, the spliced composite section defined mainly by MST measurements is not entirely covered by OSU-SCAT measurements. However, a SCAT-composite section could be constructed for the majority of the multiple-hole intervals. For shipboard analysis, the raw data were converted to percent reflectance and averaged into four 100-nm-wide bands defined as UV (250–350 nm), blue (450–550 nm), red (650–750 nm), and nIR (850–950 nm). These bands are 50 nm wider than those used on previous ODP legs to allow integration of a greater fraction of the spectral signal. As an aid to defining lithostratigraphic units we employed the red band, which is near the instrument's maximum response. This band was also used as an aid in constructing composite sections (see "Composite Depths," p. 3). The blue band was used for comparison to shipboard measurements of the carbonate content of sediment (carbonate has a somewhat higher reflectance at this wavelength than at longer wavelengths; see Mix et al., 1992).

During shipboard analysis, it was noted that the reflectance values from the Minolta CM-2002 were consistently offset and of lower amplitude than reflectance measurements generated with the OSU-SCAT system. Possible explanations for the offset were differences in the calibrations of the two instruments and the use of Glad plastic wrap over cores when working with the CM-2002 to protect its integrating sphere and glass lens. The CM-2002 employs a two-point calibration using a white ceramic transfer standard and a black-light trap to set the full range of the instrument. In contrast, the OSU-SCAT system measures internal white and black-trap standards with each sample and corrects for reflectance caused by imperfections in the integrating sphere using four external Spectralon standards with nominal reflectance of 2%, 40%, 75% and 100%. To intercalibrate the two instruments, we

repeatedly measured the OSU-SCAT's external standards using the CM-2002 (n = 20 for each standard). The results demonstrate that the Minolta CM-2002 in SCE mode generates reflectance values that are consistently lower (by ~7%–8%) than those obtained from the OSU-SCAT (Fig. **F12**). The effect of using Glad wrap was to increase the reflectivity of the 2% standard to ~4% (effectively acting as a mirror) and to decrease the reflectance of the brighter standards. The Glad-wrap effect was smaller than the calibration offset between the two instruments. The data from the Minolta instrument are presented in uncorrected form in this volume. Postcruise work will focus on determining spectrally resolved correction factors to enable direct comparison of the Minolta and OSU-SCAT instruments in the visible wavelength range.

F12. Intercalibration between the OSU-SCAT and Minolta CM-2002 spectrophotometers, **p. 47.**

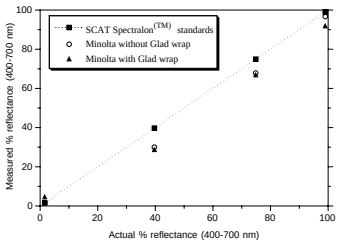

Resistivity

Measurements of sediment resistivity were generated by the OSU-SCAT every 4–6 cm in split core sections. (see **"Reflectance,"** p. 23). The resistivity meter consists of two Wenner-type arrays (channels A and B) located on opposite sides of the landing board of the OSU-SCAT's integration sphere (Fig. **F13**) Each array is aligned in the direction of the core's long axis, and consists of four electrodes that penetrate the sediment to a depth of ~0.5 cm. A ± 0.3-V, 980-Hz sine wave is applied to the outer electrodes, and the current through the sediment is measured. The inner electrodes are used to measure the drop in potential. A measure of resistivity (R_0) is then obtained through the relationship:

$$R_0 = V/I \times C, \quad (3)$$

where V is the voltage, I is the current, and C is an empirically derived "cell constant" that is a function of the cross-sectional area and length of sample through which the current passes. Calibration of the OSU-SCAT resistivity meter in synthetic water samples yielded a cell constant of C = 0.9. The resistivity is then expressed in units of Ωm. Since resistivity is dependent on temperature (as temperature increases resistivity decreases), the temperature of the sediment must be recorded at the same time as resistivity measurements are made. The OSU-SCAT landing board has two temperature probes (Fig. **F13**), thereby allowing correction to 20ºC using the following empirical relationship:

$$R_0 = R_t \cdot [1 + 0.025 \cdot (T - 20)]. \quad (4)$$

If the resistivity of the mineral particles is very large compared with the interstitial water, then the proportion of the current carried by the minerals can be ignored. The conductivity of ocean water is approximately 10 orders of magnitude larger than that of silicate minerals. Because water has such a large effect, it is assumed that measurements are made under saturated conditions; therefore, precautions need to be taken to minimize core drying after splitting, such as covering exposed sections with plastic wrap. The resistivity measured at any given depth will depend on the volume fractions of the sedimentary constituents, their individual conductivities, and the sedimentary microstructure. Empirical relationships can account for these variations using a variation of Archie's Law (Archie, 1942; Boyce, 1968):

F13. Schematic diagram of the landing board on the OSU-SCAT's integration sphere, **p. 48.**

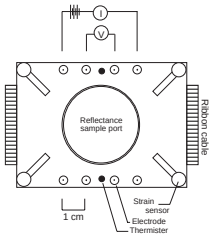

$$F = a\Phi^{-m}, \quad (5)$$

$$F = R_0/R_w, \quad (6)$$

where F is the formation factor, Φ is the porosity fraction, a is a proportionality constant, and m is a constant that is a function of the particular lithology. The formation factor for a particular lithology represents the reduction in brine conductivity, caused by the presence of an insulating phase (sediment), and is related to the porosity and the tortuosity, which represents the fluid path around the solid grains and the interconnectivity of the pore spaces. The formation factor is expressed as the ratio of the temperature-corrected resistivity of the saturated sediment (R_0) to that of the interstitial water (R_w). The interstitial water is assumed to be standard seawater with a salinity of 35‰ at 20°C, and has a resistivity of 0.209 Ωm (i.e., $R_w = [2.803 + 0.0996 \cdot T]^{-1}$).

If resistivity and porosity data are both available from the same sediment sample (e.g., the discrete-sample porosities measured by the MAD method), then an exponential fit to a plot of the formation factor (from Eq. 6) vs. porosity can be used to estimate the a and m constants in Equation 5.

Resistivity can also be used to estimate diffusion coefficients for ionic species. In principle, the manner in which saturated sediments transmit electrical current is analogous to their ability to permit molecular diffusion. The diffusivity of dissolved species within sediments is a function of the species themselves, the temperature, the porosity, and the tortuosity (geometry) of the free channels in the sediment. Therefore, the diffusion coefficient (d) of a given molecule or ionic species within the sediment is given by

$$d = d_o/F, \quad (7)$$

where d_o is the diffusion coefficient for the given species in free solution at a given temperature and ionic strength, and F is the formation factor. If the sediments contain a high concentration of clay minerals, however, then the clay can conduct a significant part of the current and will result in artificially high diffusion coefficients. The low clay mineral concentrations in most Leg 177 cores suggest that resistivity may provide a means of approximating diffusion coefficients in siliceous and carbonate oozes.

The high-resolution resistivity data collected during Leg 177 generally have a high signal-to-noise ratio, although periodic technical problems with the lander assembly did result in data from one or more of the channels being compromised temporarily until the problem was rectified. There was also a consistent offset between the A and B channels of ~0.2 Ωm, and channel A sometimes showed an inverse correlation with channel B, even during calibration runs in seawater. This may be an electronic problem with amplification of the A channel signal. As a consequence, only data from the B channel are shown in this volume. Data from the B channel show an excellent correlation with the GRA bulk density and an anti-correlation with discrete sample (MAD method) porosities (see "Physical Properties" sections in the site chapters).

Postcruise analysis of the resistivity data will first involve further evaluation of their quality and a diagnosis of the problem with the A channel. This will hopefully allow correction of the A channel data and

an improved signal-to-noise ratio. Resistivity measurements will then be used in conjunction with spectral reflectance and whole-core logging data from the MST, to investigate sediment mineralogy and fabric.

DOWNHOLE MEASUREMENTS

Introduction

Downhole logs are used to directly determine the in situ physical, chemical, and structural properties of sediments penetrated by drilling. Continuous downhole measurements complement discrete measurements obtained from cores and serve as a proxy for physical and sedimentological properties where core recovery is incomplete. In addition, by correlating core and downhole measurements, the true stratigraphic depth of core material can be determined. By mapping the sediments to the borehole depth, as determined by the wireline, it is also possible to estimate postcoring sediment expansion.

During Leg 177, we used the triple combination and the geological high-sensitivity magnetic tool (GHMT) strings to log Hole 1093D. In addition, the Lamont temperature logging tool (TLT) was deployed to recover borehole temperature changes. The tools were run at the highest resolution allowable to record cyclicity on the shortest possible time scale, in accord with the paleoceanographic objectives of the leg (Table T7).

ODP wireline logging services aboard the *JOIDES Resolution* are provided by the LDEO-BRG and Schlumberger Well Logging Services. The tools have been modified for use in a 3.8-in drill-string bore.

T7. Specifications of the downhole tools deployed during Leg 177, p. 57.

Logging Tools

A brief description of logging tools used by LDEO-BRG is found in the Wireline Logging Service Guide (1994). A more thorough discussion of logging sensor principles and their geologic applications can be found in Serra (1984), Timur and Toksöz (1985), Ellis (1987), and Schlumberger (1989). A description of the GHMT sensors can be found in the ODP Leg 162 *Initial Reports* volume (Jansen, Raymo, Blum, et al., 1996) and Schlumberger (1994). A summary of the typical vertical resolution of the tools used during Leg 177 is provided in Table T7.

The triple combination tool string consists of a hostile environment natural gamma-ray sonde (HNGS), an accelerator porosity sonde (APS), a hostile environment litho-density sonde (HLDS), and a dual induction tool (DIT). In addition, the TLT is run as part of the triple combination tool string. The GHMT string is composed of the nuclear magnetic resonance tool (NMRT), which measures the total magnetic field, and the susceptibility magnetic tool (SUMT). A natural gamma-ray spectrometry tool (NGT) is also run as part of the GHMT string.

Logging Operations

After coring is completed, the hole is flushed with heavy viscous drilling fluid to clear sediment fill and condition the hole for logging. The bottom-hole assembly is then pulled up to logging depth. If obstructions occur on the upward trip, or if bridging is expected to cause a problem, a wiper trip may occur where the pipe is lowered to the bottom of the hole and then brought up to logging depth. Finally,

the tool strings are lowered into the hole by a seven-conductor wireline cable that transmits the data back to the Schlumberger Multitask Acquisition and Imaging System (MAXIS 500) logging computers where logging data are monitored and recorded in real time. The wireline heave-motion compensator may be employed in rough seas to minimize the effect of ship heave on tool position within the hole. After logging and initial shipboard processing, the data are transmitted back to LDEO-BRG for shore-based processing and corrections. A shore-based log processing report is provided in the **"Site 1093"** chapter.

Data Quality

The quality of the log data is dependent primarily on borehole conditions. Large-diameter or irregular boreholes can lead to problems with measurements that require good contact with the borehole wall, such as density and porosity. Natural gamma-ray measurements can also be affected by the size and variability of the borehole. Measurements that have deeper investigation depths, such as resistivity, are less sensitive to variations in borehole size. The quality of the borehole is generally better if circulation of drilling fluid can be minimized and if a young hole or a dedicated hole, which has been drilled immediately before logging, can be used.

REFERENCES

Abelmann, A., 1992. Early to middle Miocene radiolarian stratigraphy of the Kerguelen Plateau, Leg 120. *In* Wise, S.W., Jr., Schlich, R., et al., *Proc. ODP, Sci. Results,* 120: College Station, TX (Ocean Drilling Program), 757–783.

Archie, G.E., 1942. The electrical resistivity log as an aid in determining some reservoir characteristics. *Trans. Am. Inst. Min. Metall. Pet. Eng.,* 146:54–62.

Backman, J., and Raffi, I., 1997. Calibration of Miocene nannofossil events to orbitally tuned cyclostratigraphies from Ceara Rise. *In* Shackleton, N.J., Curry, W.B., Richter, C., and Bralower, T.J. (Eds.), *Proc. ODP, Sci. Results*, 154: College Station, TX (Ocean Drilling Program), 83–99.

Baldauf, J.G., and Barron, J.A., 1991. Diatom biostratigraphy: Kerguelen Plateau and Prydz Bay regions of the Southern Ocean. *In* Barron, J., Larsen, B., et al., *Proc. ODP, Sci. Results,* 119: College Station, TX (Ocean Drilling Program), 547–598.

Barron, J.A., 1992. Neogene diatom datum levels in the equatorial and North Pacific. *In* Ishizaki, K., and Saito, T. (Eds.), *The Centenary of Japanese Micropaleontology:* Tokyo (Terra Sci. Publ.), 413–425.

Barron, J.A., Baldauf, J.G., Barrera, E., Caulet, J.-P., Huber, B.T., Keating, B.H., Lazarus, D., Sakai, H., Thierstein, H.R., and Wei, W., 1991. Biochronologic and magnetochronologic synthesis of Leg 119 sediments from the Kerguelen Plateau and Prydz Bay, Antarctica. *In* Barron, J., Larsen, B., et al., *Proc. ODP, Sci. Results,* 119: College Station, TX (Ocean Drilling Program), 813–847.

Berggren, W.A., 1992a. Neogene planktonic foraminifer magnetobiostratigraphy of the southern Kerguelen Plateau (Sites 747, 748, and 751). *In* Wise, S.W., Jr., Schlich, R., et al., *Proc. ODP, Sci. Results,* 120 (Pt. 2): College Station, TX (Ocean Drilling Program), 631–647.

————, 1992b. Paleogene planktonic foraminifer magnetobiostratigraphy of the Southern Kerguelen Plateau (Sites 747–749). *In* Wise, S.W., Jr., Schlich, R., et al., *Proc. ODP, Sci. Results,* 120 (Pt. 2): College Station, TX (Ocean Drilling Program), 551–568.

Berggren, W.A., and Aubert J., 1983. Paleogene benthonic foraminiferal biostratigraphy and bathymetry of the Central Coast Ranges of California. *In* Brabb, E.E. (Ed.), *Studies in Tertiary Stratigraphy of the California Coast Ranges*. Geol. Surv. Prof. Pap. U.S., 1213:4–21.

Berggren, W.A., Hilgen, F.J., Langereis, C.G., Kent, D.V., Obradovich, J.D., Raffi, I., Raymo, M.E., and Shackleton, N.J., 1995a. Late Neogene chronology: new perspectives in high-resolution stratigraphy. *Geol. Soc. Am. Bull.,* 107:1272–1287.

Berggren, W.A., Kent, D.V., Swisher, C.C., III, and Aubry, M.-P., 1995b. A revised Cenozoic geochronology and chronostratigraphy. *In* Berggren, W.A., Kent, D.V., Aubry, M.-P., and Hardenbol, J. (Eds.), *Geochronology, Time Scales and Global Stratigraphic Correlation*. Spec. Publ.—Soc. Econ. Paleontol. Mineral. (Soc. Sediment. Geol.), 54:129–212.

Blum, P., 1997. Physical Properties Handbook: a Guide to the Shipboard Measurements of Physical Properties of Deep-sea Cores. *ODP Tech. Note,* 26.

Boyce, R.E., 1968. Electrical resistivity of modern marine sediments from the Bering Sea. *J. Geophys. Res.,* 73:4759–4766.

Brunner, C.A., 1991. Latest Miocene to Quaternary biostratigraphy and paleoceanography, Site 704, subantarctic South Atlantic Ocean. *In* Ciesielski, P.F., Kristoffersen, Y., et al., *Proc. ODP, Sci. Results,* 114: College Station, TX (Ocean Drilling Program), 201–215.

Bukry, D., 1973. Low-latitude coccolith biostratigraphic zonation. *In* Edgar, N.T., Saunders, J.B., et al., *Init. Repts. DSDP,* 15: Washington (U.S. Govt. Printing Office), 685–703.

————, 1975. Coccolith and silicoflagellate stratigraphy, northwestern Pacific Ocean, Deep Sea Drilling Project Leg 32. *In* Larson, R.L., Moberly, R., et al., *Init. Repts. DSDP,* 32: Washington (U.S. Govt. Printing Office), 677–701.

Cande, S.C., and Kent, D.V., 1995. Revised calibration of the geomagnetic polarity timescale for the Late Cretaceous and Cenozoic. *J. Geophys. Res.,* 100:6093–6095.

Caulet, J.-P., 1991. Radiolarians from the Kerguelen Plateau, Leg 119. *In* Barron, J., Larsen, B., et al., *Proc. ODP, Sci. Results,* 119: College Station, TX (Ocean Drilling Program), 513–546.

Crux, J.A., 1991. Calcareous nannofossils recovered by Leg 114 in the subantarctic South Atlantic Ocean. *In* Ciesielski, P.F., Kristoffersen, Y., et al., *Proc. ODP, Sci. Results,* 114: College Station, TX (Ocean Drilling Program), 155–177.

Curry, W.B., Shackleton, N.J., Richter, C., et al., 1995. *Proc. ODP, Init. Repts.,* 154: College Station, TX (Ocean Drilling Program).

Davis, E.E., Mottl, M.J., Fisher, A.T., et al., 1992. *Proc. ODP, Init. Repts.,* 139: College Station, TX (Ocean Drilling Program).

Eisma, D., and Van der Gaast, S.J., 1971. Determination of opal in marine sediments by X-ray diffraction. *Neth. J. Sea Res.*, 5:382–389.

Ellis, D.V., 1987. *Well Logging for Earth Scientists:* New York (Elsevier).

Emeis, K.-C., and Kvenvolden, K.A., 1986. Shipboard organic geochemistry on *JOIDES Resolution. ODP Tech. Note,* 7.

Emerson, S., and Hedges, J.I., 1988. Processes controlling the organic carbon content of open ocean sediments. *Paleoceanography,* 3:621–634.

Farrell, J.W., and Janecek, T.R., 1991. Late Neogene paleoceanography and paleoclimatology of the northeast Indian Ocean (Site 758). *In* Weissel, J., Peirce, J., Taylor, E., Alt, J., et al., *Proc. ODP, Sci. Results,* 121: College Station, TX (Ocean Drilling Program), 297–355.

Fenner, J., 1984. Eocene-Oligocene planktic diatom stratigraphy in the low latitudes and the high southern latitudes. *Micropaleontology,* 30:319–342.

Foreman, H.P., 1975. Radiolaria from the North Pacific, Deep Sea Drilling Project, Leg 32. *In* Larson, R.L., Moberly, R., et al., *Init. Repts. DSDP,* 32: Washington (U.S. Govt. Printing Office), 579–676.

Gartner, S., 1977. Calcareous nannofossil biostratigraphy and revised zonation of the Pleistocene. *Mar. Micropaleontol.,* 2:1–25.

————, 1990. Neogene calcareous nannofossil biostratigraphy, Leg 116 (Central Indian Ocean). *In* Cochran, J.R., Stow, D.A.V., et al., *Proc. ODP, Sci. Results,* 116: College Station, TX (Ocean Drilling Program), 165–187.

————, 1992. Miocene nannofossil chronology in the North Atlantic, DSDP Site 608. *Mar. Micropaleontol.,* 18:307–331.

Gersonde, R., Abelmann, A., Burckle, L.H., Hamilton, N., Lazarus, D., McCartney, K., O'Brien, P., Spieß, V., and Wise, S.W., Jr., 1990. Biostratigraphic synthesis of Neogene siliceous microfossils from the Antarctic Ocean, ODP Leg 113 (Weddell Sea). *In* Barker, P.F., Kennett, J.P., et al., *Proc. ODP, Sci. Results,* 113: College Station, TX (Ocean Drilling Program), 915–936.

Gersonde, R., and Bárcena, M.A., 1998. Revision of the late Pliocene–Pleistocene diatom biostratigraphy for the northern belt of the Southern Ocean. *Micropaleontology,* 44:1–15.

Gersonde, R., and Burckle, L.H., 1990. Neogene diatom biostratigraphy of ODP Leg 113, Weddell Sea (Antarctic Ocean). *In* Barker, P.F., Kennett, J.P., et al., *Proc. ODP, Sci. Results,* 113: College Station, TX (Ocean Drilling Program), 761–789.

Gersonde, R., Spiess, V., Flores, J. A., Hagen, R., and Kuhn, G., 1998. The sediments of Gunnerus Ridge and Kainan Maru Seamount (Indian sector of Southern Ocean). *Deep-Sea Res. Part I,* 45:1515–1540.

Gieskes, J.M., Gamo, T., and Brumsack, H., 1991. Chemical methods for interstitial water analysis aboard *JOIDES Resolution. ODP Tech. Note,* 15.

Gombos, A.M., Jr., 1983. Middle Eocene diatoms from the South Atlantic. *In* Ludwig, W.J., Krasheninnikov, V.A., et al., *Init. Repts. DSDP,* 71 (Pt. 1): Washington (U.S. Govt. Printing Office), 565–582.

Gombos, A.M., Jr., and Ciesielski, P.F., 1983. Late Eocene to early Miocene diatoms from the southwest Atlantic. *In* Ludwig, W.J., Krasheninnikov, V.A., et al., *Init. Repts. DSDP,* 71 (Pt. 2): Washington (U.S. Govt. Printing Office), 583–634.

Hagelberg, T.K., Pisias, N.G., Shackleton, N.J., Mix, A.C., and Harris, S., 1995. Refinement of a high-resolution, continuous sedimentary section for studying equatorial Pacific Ocean paleoceanography, Leg 138. *In* Pisias, N.G., Mayer, L.A., Janecek, T.R., Palmer-Julson, A., and van Andel, T.H. (Eds.), *Proc. ODP, Sci Results,* 138: College Station, TX (Ocean Drilling Program), 31–46.

Hagelberg, T., Shackleton, N., Pisias, N., and Shipboard Scientific Party, 1992. Development of composite depth sections for Sites 844 through 854. *In* Mayer, L., Pisias, N., Janecek, T., et al., *Proc. ODP, Init. Repts.,* 138 (Pt. 1): College Station, TX (Ocean Drilling Program), 79–85.

Harwood, D.M., Lazarus, D.B., Abelmann, A., Aubry, M.-P., Berggren, W.A., Heider, F., Inokuchi, H., Maruyama, T., McCartney, K., Wei, W., and Wise, S.W., Jr., 1992. Neogene integrated magnetobiostratigraphy of the central Kerguelen Plateau, Leg 120. *In* Wise, S.W., Jr., Schlich, R., et al., *Proc. ODP, Sci. Results,* 120: College Station, TX (Ocean Drilling Program), 1031–1052.

Harwood, D.M., and Maruyama, T., 1992. Middle Eocene to Pleistocene diatom biostratigraphy of Southern Ocean sediments from the Kerguelen Plateau, Leg 120. *In* Wise, S.W., Jr., Schlich, R., et al., *Proc. ODP, Sci. Results,* 120: College Station, TX (Ocean Drilling Program), 683–733.

Hempel, P., and Bohrmann, G., 1990. Carbonate-free sediment components and aspects of silica diagenesis at Sites 707, 709, and 711 (Leg 115, western Indian Ocean). *In* Duncan, R.A., Buckman, J., Peterson, L.C., et al., *Proc. ODP, Sci. Results,* 115: College Station, TX (Ocean Drilling Program), 677–698.

Jansen, E., Raymo, M.E., Blum, P., et al., 1996. *Proc. ODP, Init. Repts.,* 162: College Station, TX (Ocean Drilling Program).

Jenkins, D.G., and Srinivasan, M.S., 1986. Cenozoic planktonic foraminifers from the equator to the sub-antarctic of the southwest Pacific. *In* Kennett, J.P., von der Borch, C.C., et al., *Init. Repts. DSDP,* 90: Washington (U.S. Govt. Printing Office), 795–834.

Johnson, D.A., Schneider, D.A., Nigrini, C.A., Caulet, J.-P., and Kent, D.V., 1989. Pliocene-Pleistocene radiolarian events and magnetostratigraphic calibrations for the tropical Indian Ocean. *Mar. Micropaleontol.,* 14:33–66.

Kennett, J.P., and Srinivasan, M.S., 1983. *Neogene Planktonic Foraminifera: A Phylogenetic Atlas:* Stroudsburg, PA (Hutchinson Ross).

Lamont-Doherty Earth Observatory-Borehole Research Group, 1994. *Wireline Logging Services Guide*: Lamont-Doherty Earth Observatory-Borehole Research Group.

Lazarus, D., 1992. Antarctic Neogene radiolarians from the Kerguelen Plateau, Legs 119 and 120. *In* Wise, S.W., Jr., Schlich, R., et al., *Proc. ODP, Sci. Results,* 120: College Station, TX (Ocean Drilling Program), 785–809.

Lourens, L.J., Antonarakou, A., Hilgen, F.J., Van Hoof, A.A.M., Vergnaud-Grazzini, C., and Zachariasse, W.J., 1996. Evaluation of the Plio-Pleistocene astronomical timescale. *Paleoceanography,* 11:391–413.

Lyle, M., Koizumi, I., Richter, C., et al., 1997. *Proc. ODP, Init. Repts.,* 167: College Station, TX (Ocean Drilling Program).

Mackensen, A., 1992. Neogene benthic foraminifers from the southern Indian Ocean (Kerguelen Plateau): biostratigraphy and paleoecology. *In* Wise, S.W., Jr., Schlich, R., et al., *Proc. ODP, Sci. Results,* 120: College Station, TX (Ocean Drilling Program), 649–673.

Mackensen, A., and Spiegler, D., 1992. Middle Eocene to early Pliocene *Bolboforma* (algae?) from the Kerguelen Plateau, southern Indian Ocean. *In* Wise, S.W., Jr.,

Schlich, R., et al., *Proc. ODP, Sci. Results,* 120: College Station, TX (Ocean Drilling Program), 675–682.

Manheim, F.T., and Sayles, F.L., 1974. Composition and origin of interstitial waters of marine sediments, based on deep sea drill cores. *In* Goldberg, E.D. (Ed.), *The Sea* (Vol. 5): *Marine Chemistry: The Sedimentary Cycle:* New York (Wiley), 527–568.

Martini, E., 1971. Standard Tertiary and Quaternary calcareous nannoplankton zonation. *In* Farinacci, A. (Ed.), *Proc. 2nd Int. Conf. Planktonic Microfossils Roma:* Rome (Ed. Tecnosci.), 2:739–785.

Mazzullo, J.M., Meyer, A., and Kidd, R.B., 1988. New sediment classification scheme for the Ocean Drilling Program. *In* Mazzullo, J., and Graham, A.G. (Eds.), Handbook for Shipboard Sedimentologists. *ODP Tech. Note, 8*:45–67.

Meyers, P.A., 1994. Preservation of elemental and isotopic source identification of sedimentary organic matter. *Chem. Geol.,* 144:289–302.

Mix, A.C., Rugh, W., Pisias, N.G., Veirs, S., Leg 138 Shipboard Sedimentologists (Hagelberg, T., Hovan, S., Kemp, A., Leinen, M., Levitan, M., Ravelo, C.), and Leg 138 Scientific Party, 1992. Color reflectance spectroscopy: a tool for rapid characterization of deep-sea sediments. *In* Mayer, L., Pisias, N., Janecek, T., et al., *Proc. ODP, Init. Repts.,* 138 (Pt. 1): College Station, TX (Ocean Drilling Program), 67–77.

Moore, T.C., Jr., 1995. Radiolarian stratigraphy, Leg 138. *In* Pisias, N.G., Mayer, L.A., Janecek, T.R., Palmer-Julson, A., and van Andel, T.H. (Eds.), *Proc. ODP, Sci. Results,* 138: College Station, TX (Ocean Drilling Program), 191–232.

Morley, J.J., 1985. Radiolarians from the Northwest Pacific, Deep Sea Drilling Project Leg 86. *In* Heath, G.R., Burckle, L.H., et al., *Init. Repts. DSDP,* 86: Washington (U.S. Govt. Printing Office), 399–422.

Morley, J.J., and Nigrini, C., 1995. Miocene to Pleistocene radiolarian biostratigraphy of North Pacific Sites 881, 884, 885, 886, and 887. *In* Rea, D.K., Basov, I.A., Scholl, D.W., and Allan, J.F. (Eds.), *Proc. ODP, Sci. Results,* 145: College Station, TX (Ocean Drilling Program), 55–91.

Okada, H., and Bukry, D., 1980. Supplementary modification and introduction of code numbers to the low-latitude coccolith biostratigraphic zonation (Bukry, 1973; 1975). *Mar. Micropaleontol.,* 5:321–325.

Perch-Nielsen, K., 1985. Mesozoic calcareous nannofossils. *In* Bolli, H.M., Saunders, J.B., and Perch-Nielsen, K. (Eds.), *Plankton Stratigraphy:* Cambridge (Cambridge Univ. Press), 329–426.

Pujol, C., and Bourrouilh, R., 1991. Late Miocene to Holocene Planktonic foraminifers from the subantarctic South Atlantic. *In* Ciesielski, P.F., Kristoffersen, Y., et al., *Proc. ODP, Sci. Results,* 114: College Station, TX (Ocean Drilling Program), 217–232.

Pujos, A., 1988. Spatio-temporal distribution of some Quaternary coccoliths. *Oceanol. Acta*, 11:65–77.

Qvale, G., and Spiegler, D., 1989. The stratigraphic significance of *Bolboforma* (algae, Chrysophyta) in Leg 104 samples from the Vøring Plateau. *In* Eldholm, O., Thiede, J., Taylor, E., et al., *Proc. ODP, Sci. Results,* 104: College Station, TX (Ocean Drilling Program), 487–495.

Raffi, I., Backman, J., Rio, D., and Shackleton, N.J., 1993. Plio-Pleistocene nannofossil biostratigraphy and calibration to oxygen isotopes stratigraphies from Deep Sea Drilling Project Site 607 and Ocean Drilling Program Site 677. *Paleoceanography,* 8:387–408.

Raffi, I., and Flores, J.-A., 1995. Pleistocene through Miocene calcareous nannofossils from eastern equatorial Pacific Ocean (Leg 138). *In* Pisias, N.G., Mayer, L.A., Janecek, T.R., Palmer-Julson, A., and van Andel, T.H. (Eds.), *Proc. ODP, Sci. Results,* 138: College Station, TX (Ocean Drilling Program), 233–286.

Rio, D., 1982. The fossil distribution of coccolithophore genus *Gephyrocapsa* Kamptner and related Plio-Pleistocene chronostratigraphic problems. *In* Prell, W.L., Gardner, J.V., et al., *Init. Repts. DSDP,* 68: Washington (U.S. Govt. Printing Office), 325–343.

Ruddiman, W.F., Cameron, D., and Clement, B.M., 1987. Sediment disturbance and correlation of offset holes drilled with the hydraulic piston corer: Leg 94. *In* Ruddiman, W.F., Kidd, R.B., Thomas, E., et al., *Init. Repts. DSDP,* 94 (Pt. 2): Washington (U.S. Govt. Printing Office), 615–634.

Schlumberger, 1989. *Log Interpretation Principles/Applications:* Houston, TX (Schlumberger Educ. Services).

————, 1994. *Geological High-Resolution Magnetic Tool (GHMT) Interpretation Method:* Schlumberger Riboud Product Center.

Schrader, H.J., and Gersonde, R., 1978. Diatoms and silicoflagellates. *Utrecht Micropaleontol. Bull.,* 17:129–176.

Scott, G.H., Bishop, S., and Burt, B.J., 1990. *Guide to Some Neogene Globotalids (Foraminiferida) from New Zealand*. New Zealand Geol. Surv. Paleontol. Bull., 61; New Zealand Geological Survey DSIR, Lower Hutt.

Serra, O., 1984. *Fundamentals of Well-Log Interpretation* (Vol. 1): *The Acquisition of Logging Data:* Dev. Pet. Sci., 15A: Amsterdam (Elsevier).

Shipboard Scientific Party, 1988. Explanatory notes. *In* Barker, P.F., Kennett, J.P., et al., *Proc. ODP, Init. Repts.,* 113: College Station, TX (Ocean Drilling Program), 13–32.

————, 1994. Explanatory notes. *In* Westbrook, G.K., Carson, B., Musgrave, R.J., et al., *Proc. ODP, Init. Repts.,* 146 (Pt. 1): College Station, TX (Ocean Drilling Program), 15–48.

————, 1998a. Explanatory notes. *In* Keigwin, L.D., Rio, D., Acton, G.D., et al. *Proc. ODP, Init. Repts*., 172: College Station, TX (Ocean Drilling Program), 13–29.

————, 1998b. Explanatory notes. *In* Wefer, G., Berger, W.H., Richter, C., et al., *Proc. ODP, Init. Repts.,* 175: College Station, TX (Ocean Drilling Program), 27–46.

Spiegler, D., 1991. Occurrence of *Bolboforma* (algae, Chrysophyta) in the subantarctic (Atlantic) Paleogene. *In* Ciesielski, P.F., Kristoffersen, Y., et al., *Proc. ODP, Sci. Results,* 114: College Station, TX (Ocean Drilling Program), 325–334.

Stott, L.D., and Kennett, J.P., 1990. Antarctic Paleogene planktonic foraminifer biostratigraphy: ODP Leg 113, Sites 689 and 690. *In* Barker, P.F., Kennett, J.P., et al., *Proc. ODP, Sci. Results,* 113: College Station, TX (Ocean Drilling Program), 549–569.

Takemura, A., 1992. Radiolarian Paleogene biostratigraphy in the southern Indian Ocean, Leg 120. *In* Wise, S.W., Jr., Shlich, R., et al., *Proc. ODP, Sci. Results,* 120: College Station, TX (Ocean Drilling Program), 735–756.

Takemura, A., and Ling, H.Y., 1997. Eocene and Oligocene radiolarian biostratigraphy from the Southern Ocean: correlation of ODP Legs 114 (Atlantic Ocean) and 120 (Indian Ocean). *Mar. Micropaleontol*., 30:97–116.

Thierstein, H.R., Geitzenauer, K., Molfino, B., and Shackleton, N.J., 1977. Global synchroneity of late Quaternary coccolith datum levels: validation by oxygen isotopes. *Geology,* 5:400–404.

Thomas, E., 1990. Late Cretaceous through Neogene deep-sea benthic foraminifers (Maud Rise, Weddell Sea, Antarctica). *In* Barker, P.F., Kennett, J.P., et al., *Proc. ODP, Sci. Results,* 113: College Station, TX (Ocean Drilling Program), 571–594.

Thomas, E., Barrera, E., Hamilton, N., Huber, B.T., Kennett, J.P., O'Connell, S.B., Pospichal, J.J., Speiß, V., Stott, L.D., Wei, W., and Wise, S.W., Jr., 1990. Upper Cretaceous-Paleogene stratigraphy of Sites 689 and 690, Maud Rise (Antarctica). *In* Barker, P.F., Kennett, J.P., et al., *Proc. ODP, Sci. Results,* 113: College Station, TX (Ocean Drilling Program), 901–914.

Tiedemann, R., Sarnthein, M., and Shackleton, N.J., 1994. Astronomic timescale for the Pliocene Atlantic $\delta^{18}O$ and dust flux records of Ocean Drilling Program Site 659. *Paleoceanography,* 9:619–638.

Timur, A., and Toksöz, M.N., 1985. Downhole geophysical logging. *Annu. Rev. Earth Planet. Sci.,* 13:315–344.

Von Herzen, R.P., and Maxwell, A.E., 1959. The measurement of thermal conductivity of deep-sea sediments by a needle-probe method. *J. Geophys. Res.,* 64:1557–1563.

van Morkhoven, F.P.C.M., Berggren, W.A., and Edwards, A.S., 1986. Cenozoic cosmopolitan deep-water benthic foraminifera. *Bull. Cent. Rech. Explor.—Prod. Elf-Aquitaine,* Mem. 11.

Weber, M.E., Niessen, F., Kuhn, G., and Wiedicke, M., 1997. Calibration and application of marine sedimentary physical properties using a multi-sensor core logger. *Mar. Geol.*, 136:151–172.

Wei, W., 1993. Calibration of Upper Pliocene-Lower Pleistocene nannofossil events with oxygen isotope stratigraphy. *Paleoceanography,* 8:85–99.

Wei, W., and Wise, S.W., Jr., 1990. Middle Eocene to Pleistocene calcareous nannofossils recovered by Ocean Drilling Program Leg 113 in the Weddell Sea. *In* Barker, P.F., Kennett, J.P., et al., *Proc. ODP, Sci. Results,* 113: College Station, TX (Ocean Drilling Program), 639–666.

Wentworth, C.K., 1922. A scale of grade and class terms of clastic sediments. *J. Geol.,* 30:377–392.

Wise, S.W., Jr., 1983. Mesozoic and Cenozoic calcareous nannofossils recovered by Deep Sea Drilling Project Leg 71 in the Falkland Plateau region, Southwest Atlantic Ocean. *In* Ludwig, W.J., Krasheninnikov, V.A., et al., *Init. Repts. DSDP,* 71 (Pt. 2): Washington (U.S. Govt. Printing Office), 481–550.

Figure F1. Portions of the magnetic susceptibility records from Site 1090. **A.** Cores 177-1090B-9H and 10H (left curve), 177-1090D-9H and 10H (middle curve), and 177-1090E-8H, 9H, and 10H (right curve) on the mbsf depth scale. Data from each hole are smoothed with a 5-point running mean and horizontally offset by a constant for clarity. **B.** The same cores on the mcd scale. The composite depth section has the advantage that features common to all holes are aligned.

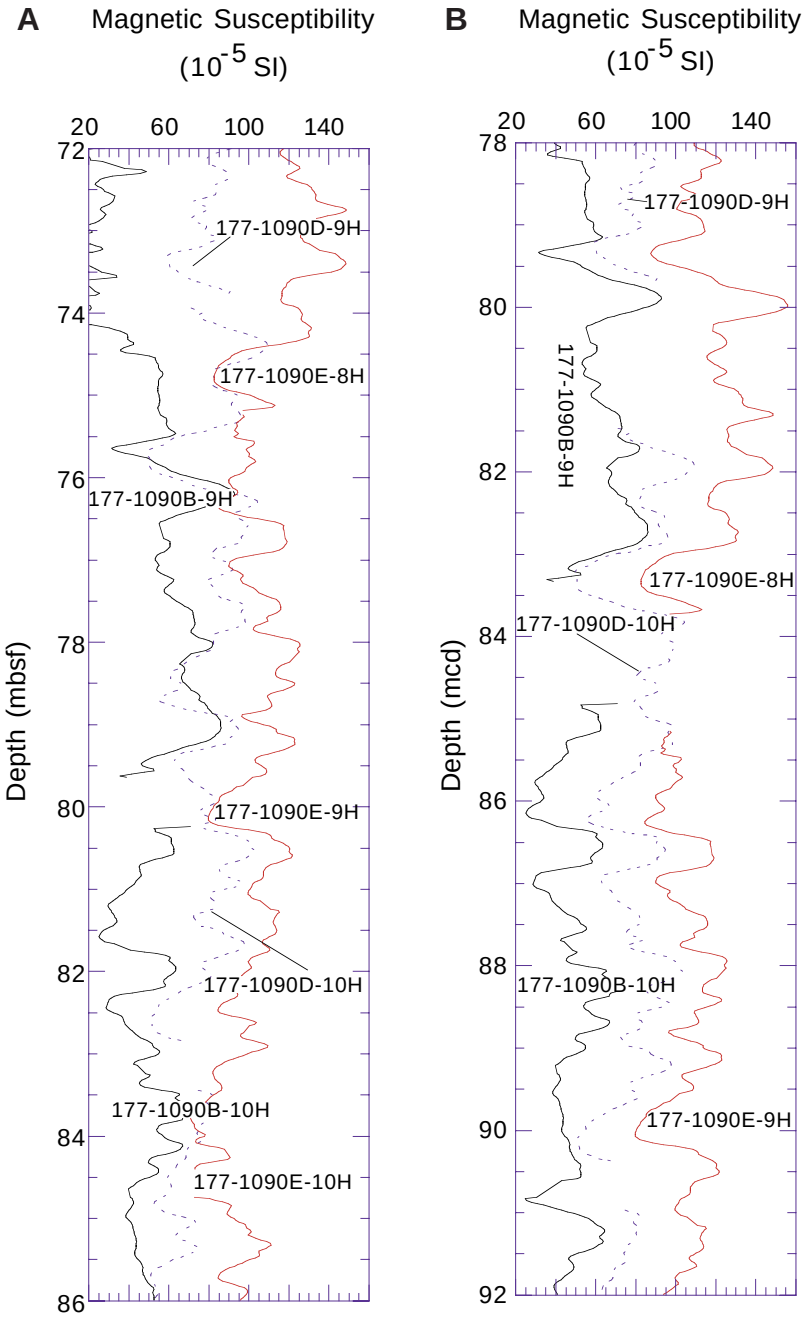

Figure F2. Portions of the spliced magnetic susceptibility record assembled from the same cores from Site 1090 that are shown in Figure F1, p. 35. Data are smoothed with a 5-point running mean and offset by a constant for clarity.

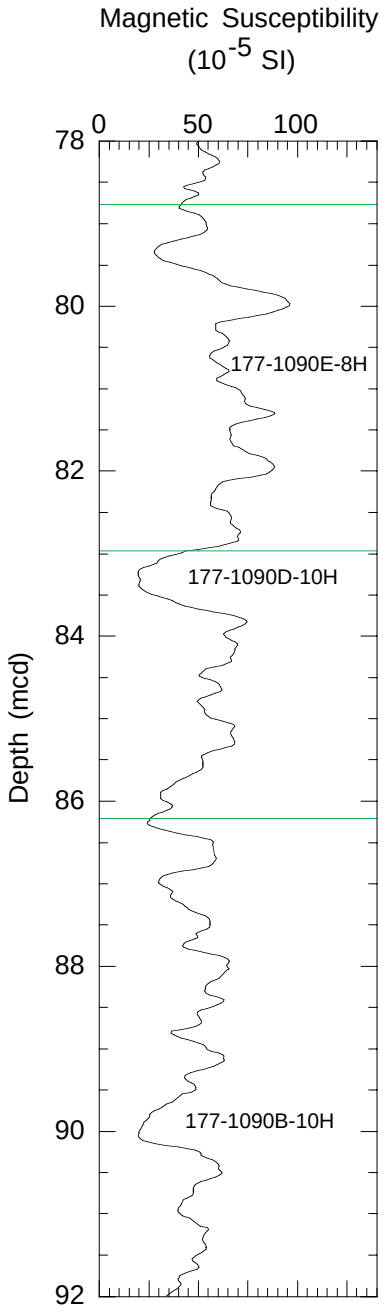

Figure F3. Example of a core description form (barrel sheet) used for sediments and sedimentary rocks in cores recovered during Leg 177. Keys for symbols are presented in Figure F4, p. 38.

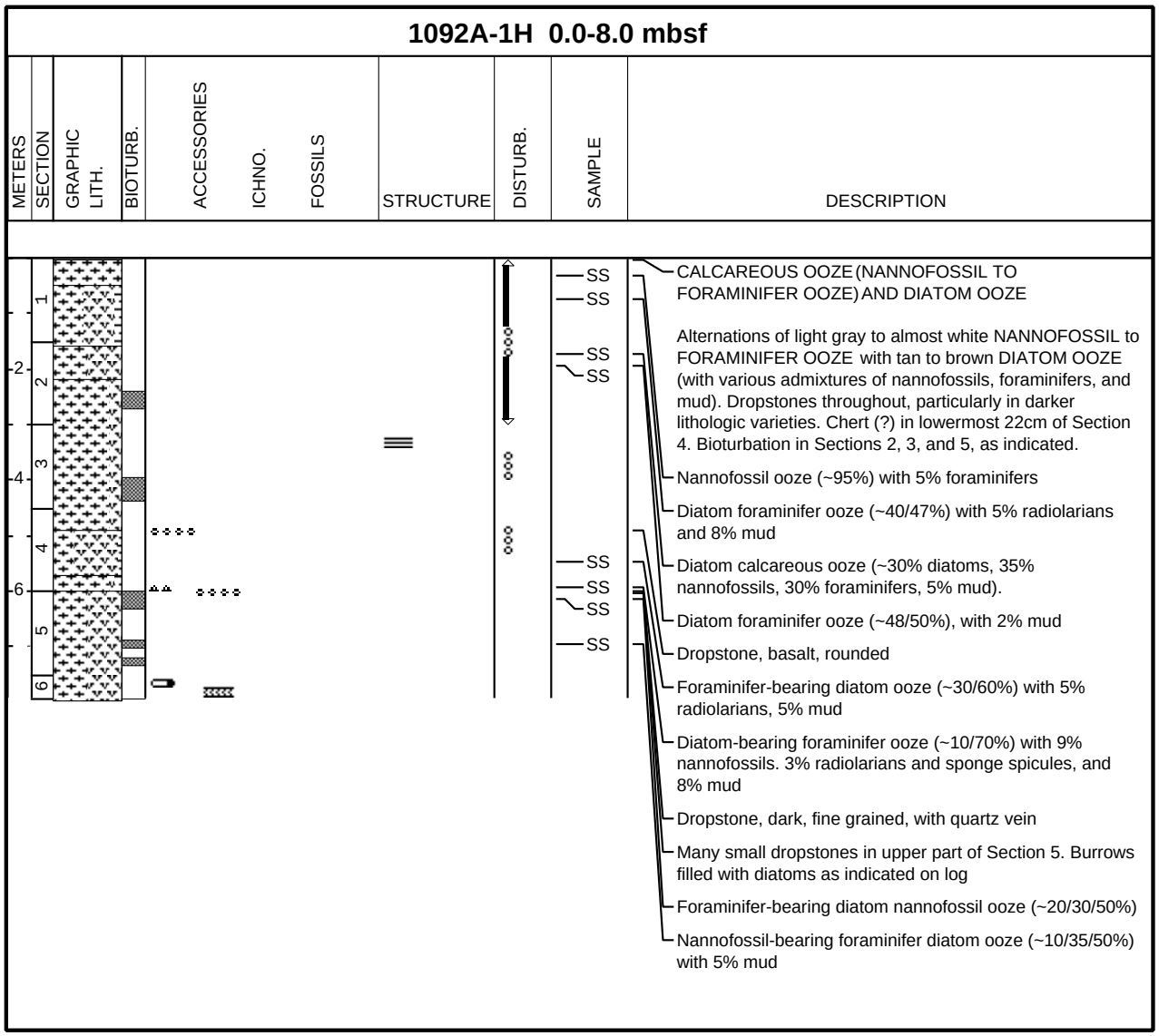

Figure F4. Patterns and symbols used in the "Lithology," "Bioturbation," "Accessories," "Fossils," "Structure," and "Disturbance" columns of the core description forms.

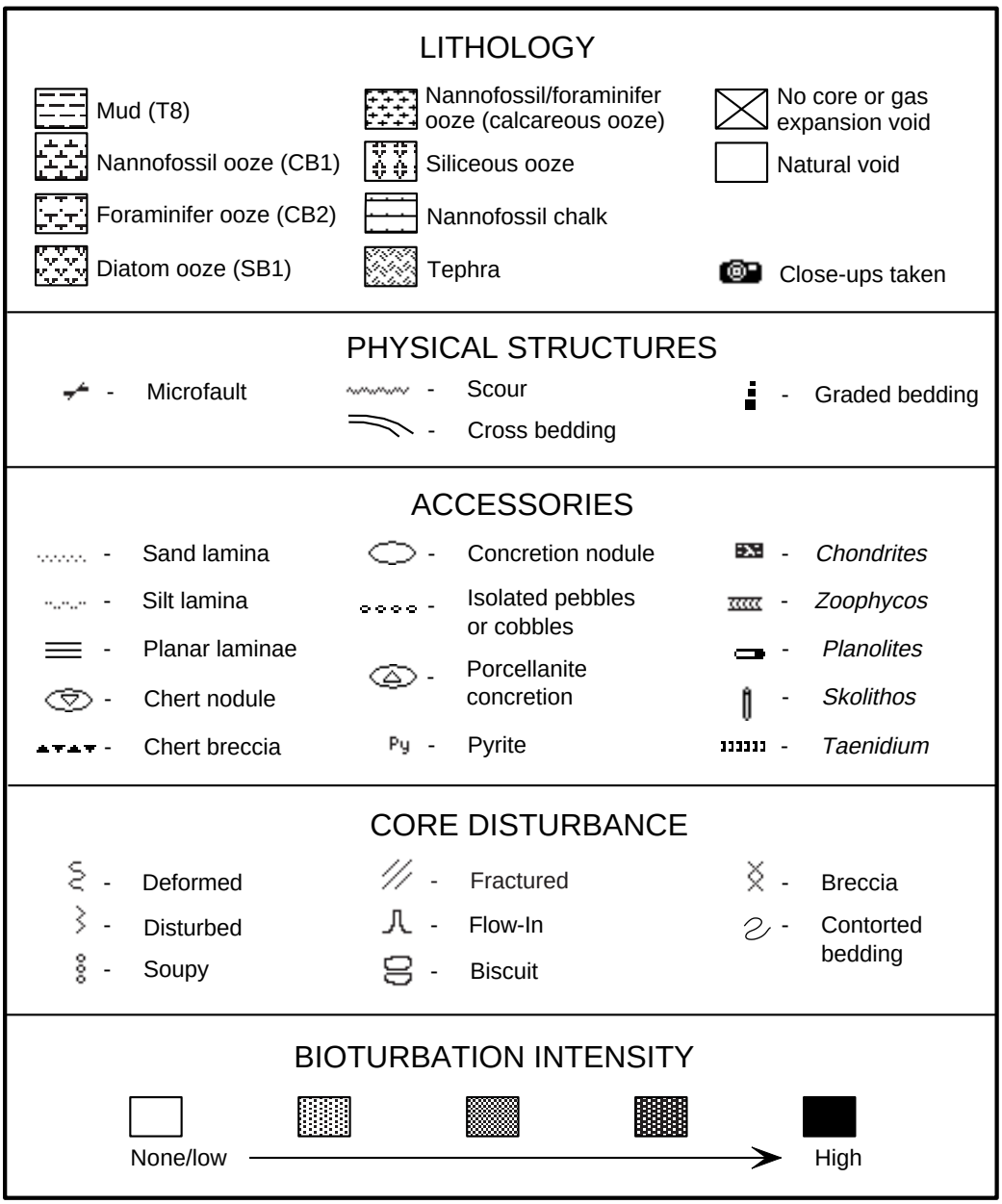

Figure F5. Linear regression between opal weight percentages and opal XRD counts inferred from XRD measurements of opal standards.

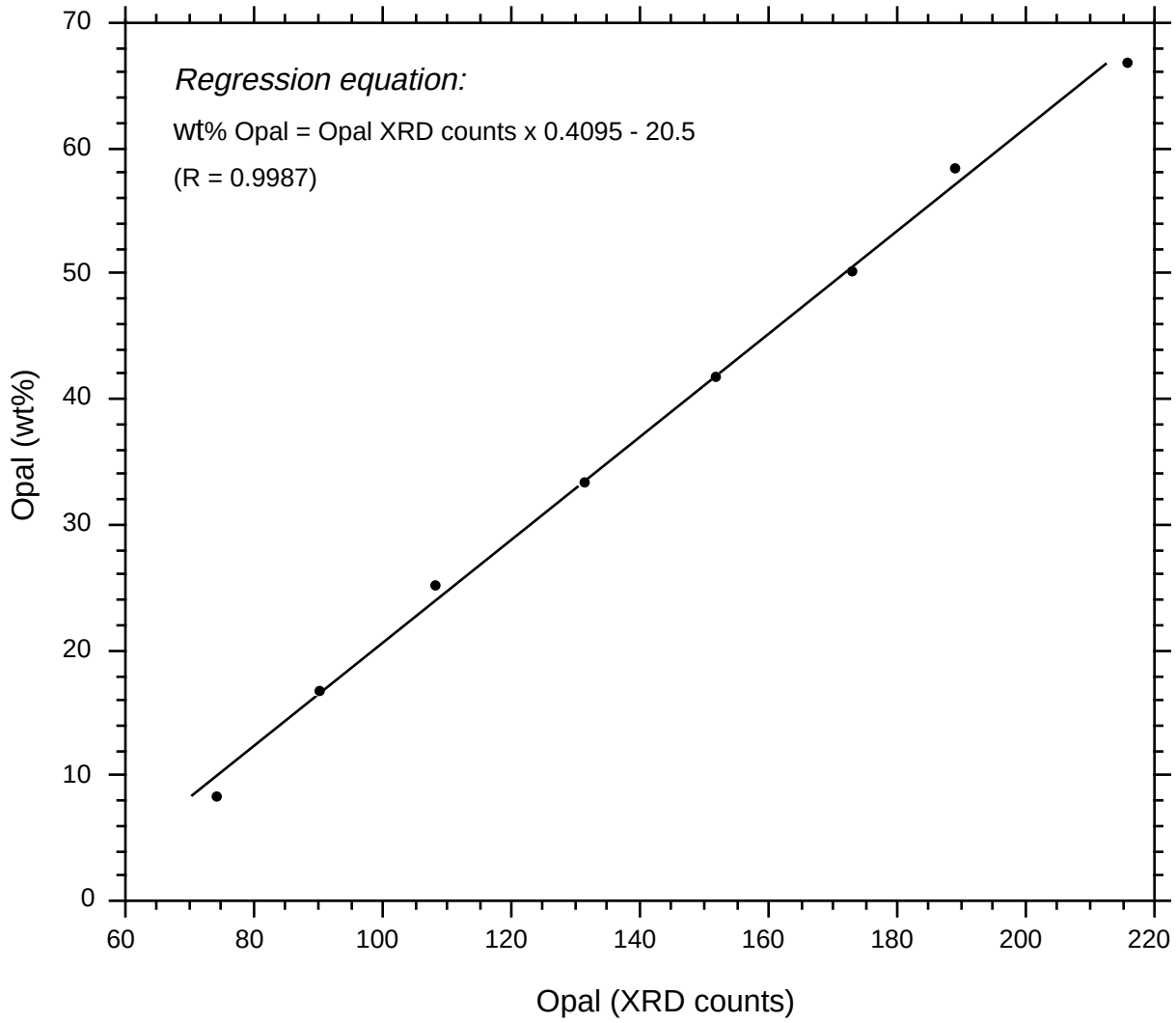

Figure F6. Combined calcareous nannofossil, planktic foraminifer, diatom, and radiolarian biostratigraphic zonal schemes tied to the geomagnetic polarity time scale (Berggren et al., 1995b), and age assignments used during Leg 177.

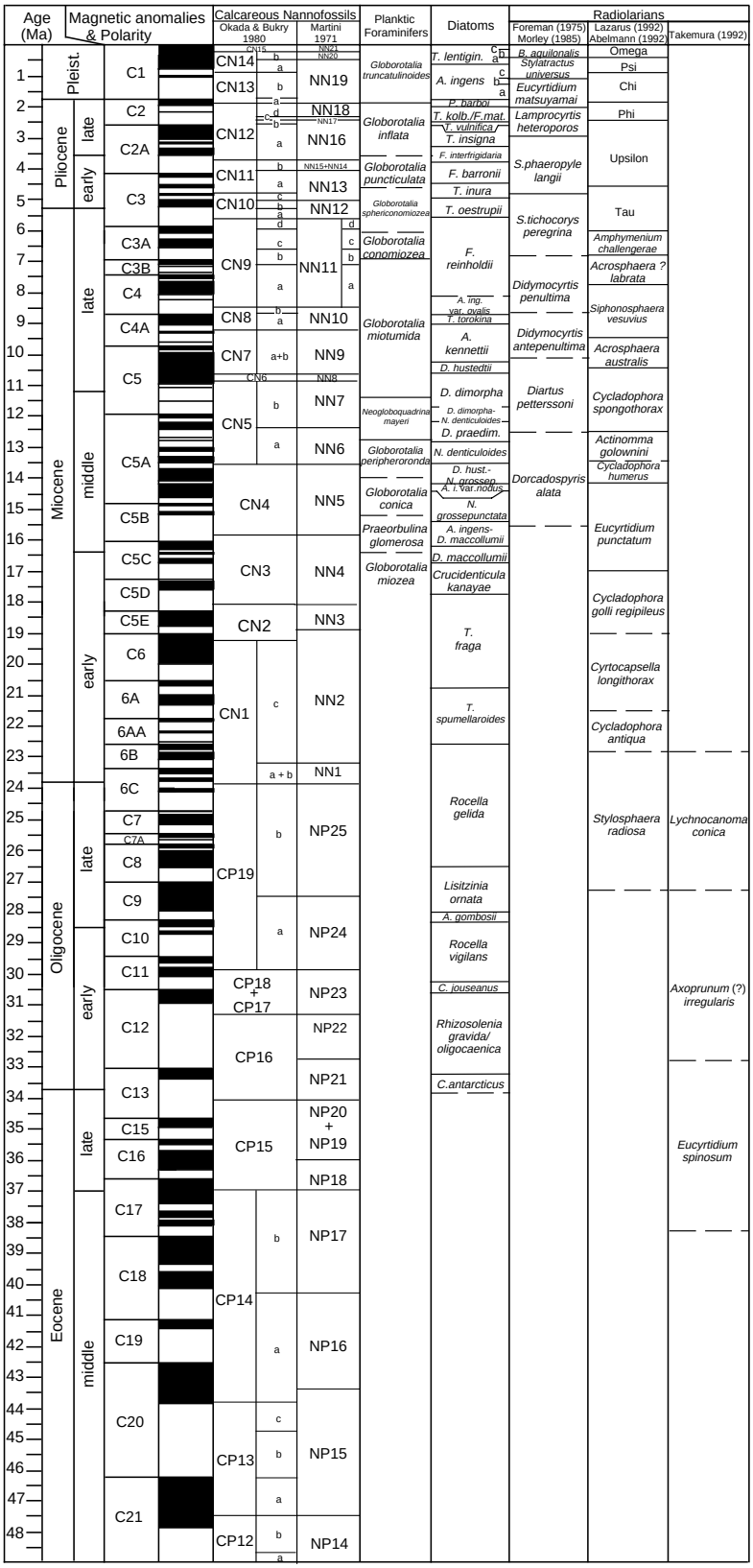

Figure F7. Geomagnetic polarity time scale of Berggren et al. (1995b), correlation of calcareous nannofossil Martini (1971) and Okada and Bukry (1980) biostratigraphic zonations, and selected datums used during Leg 177. LCO = last common occurrence. (Continued on next page.)

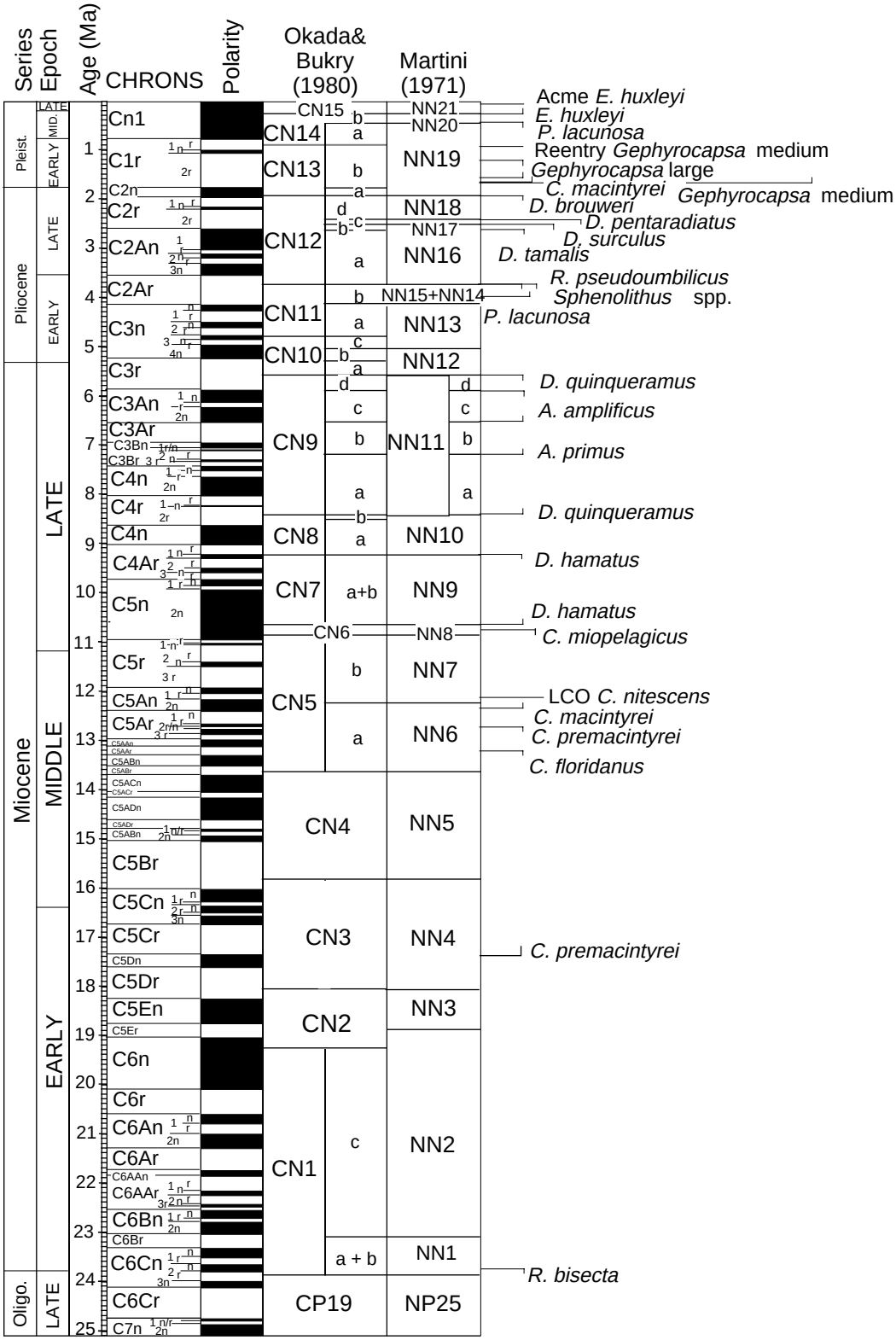

Figure F7 (continued).

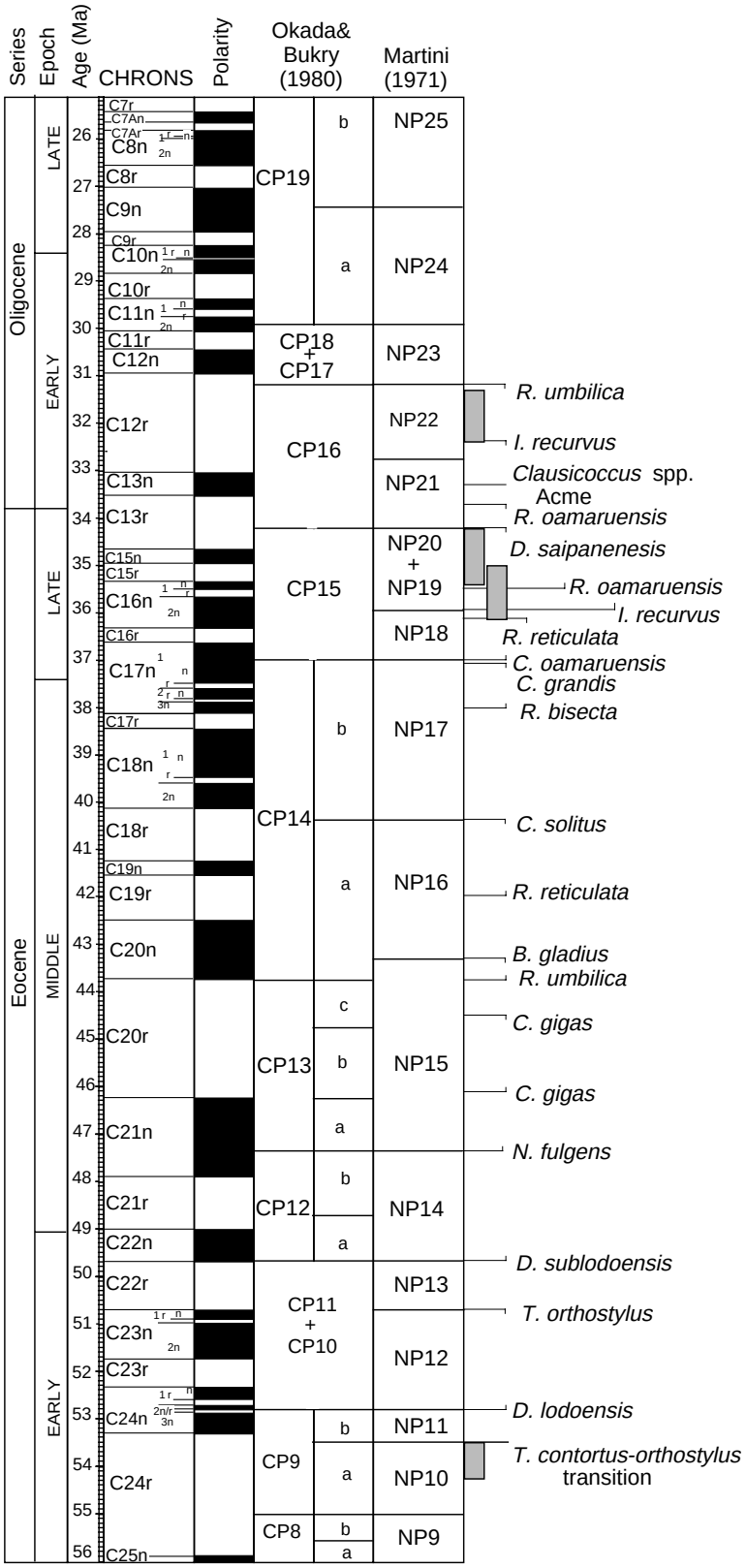

Figure F8. Plot of the number of benthic foraminifer species identified in all Leg 177 core-catcher samples vs. the number of specimens counted. All counts are based on 20-cm³ samples.

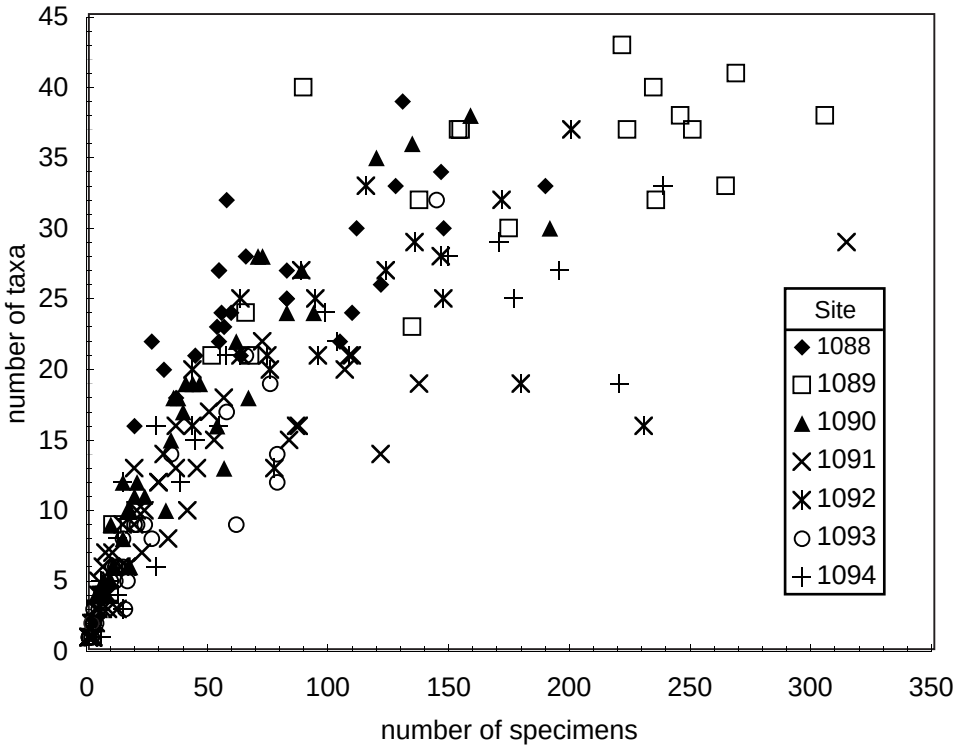

Figure F9. Diatom zonation and stratigraphic ranges of diatom species used during Leg 177 according to the compilation of Gersonde et al. (1998). * = revised zones.

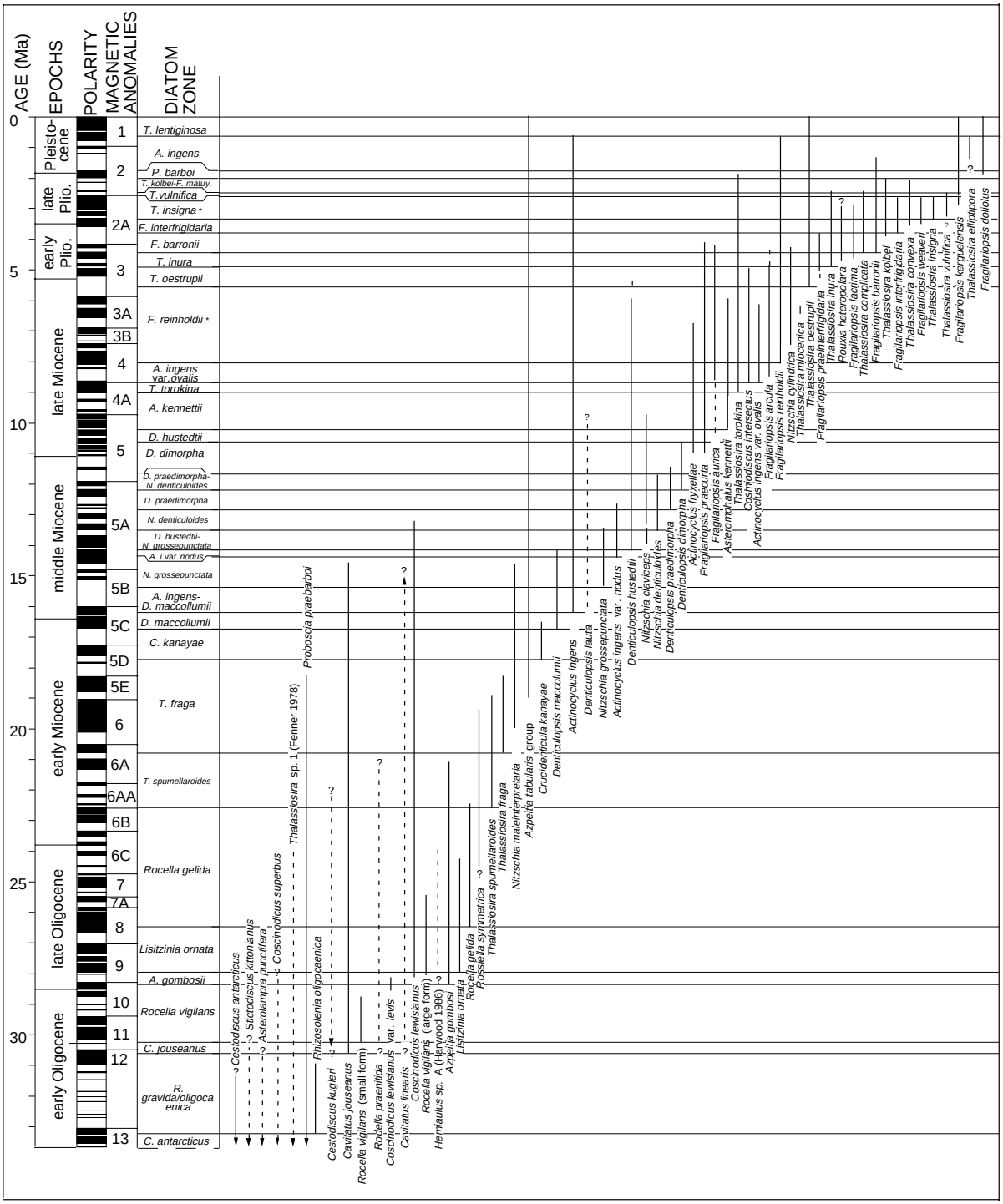

Figure F10. Water-core control measurements of total counts natural gamma-ray emission made after each section during electronic malfunction at Sites 1092 and 1093.

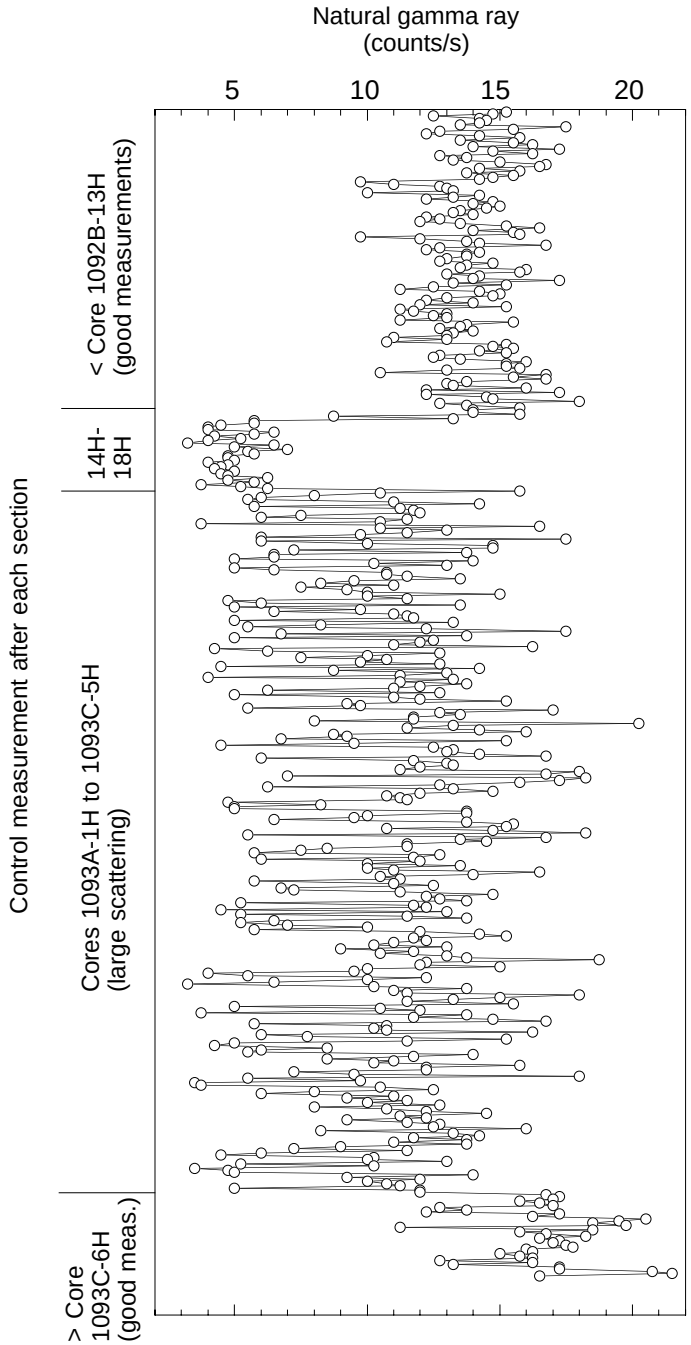

Figure F11. Comparison between oven drying and freeze-drying of samples during Leg 177.

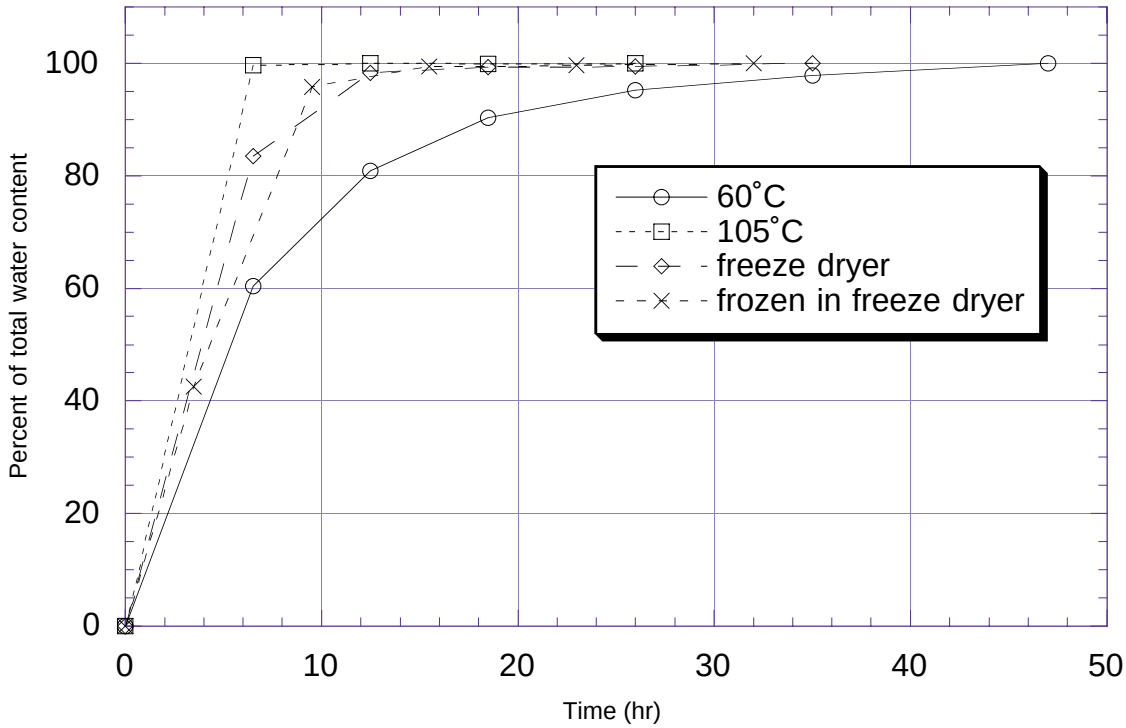

Figure F12. Intercalibration between the OSU-SCAT and Minolta CM-2002 spectrophotometers by measuring reflectance on four external Spectralon standards.

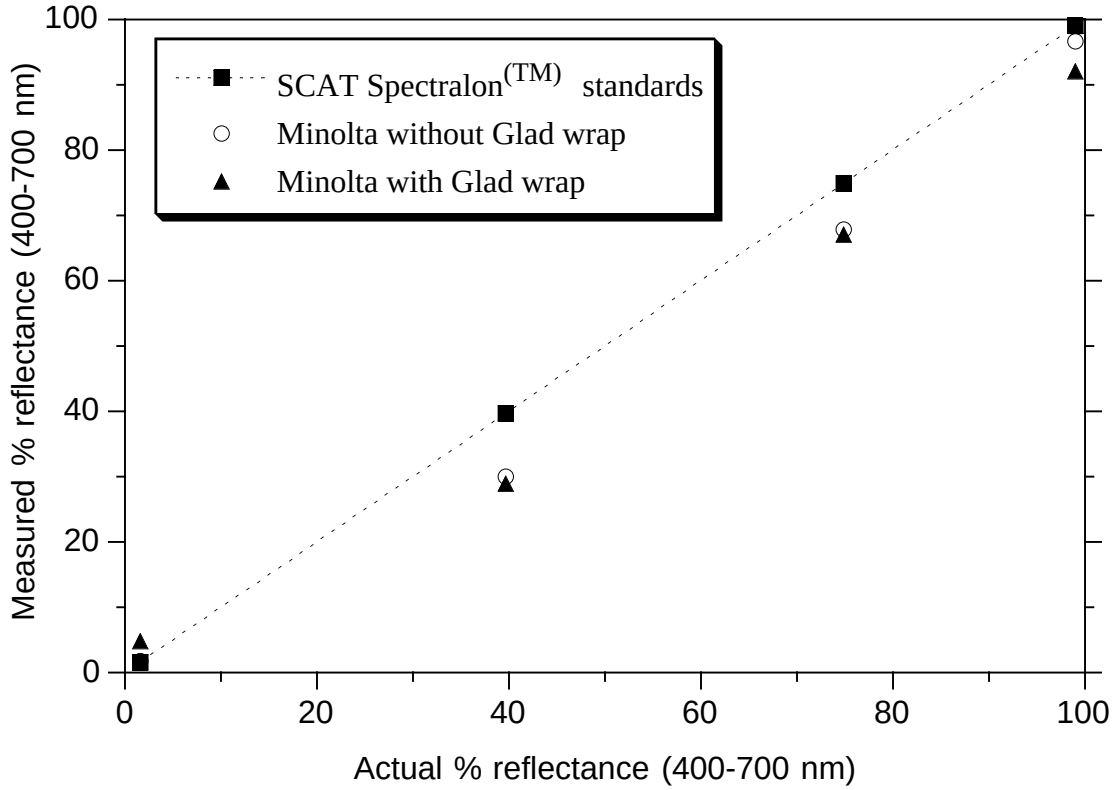

Figure F13. Schematic diagram (actual size) of the landing board on the OSU-SCAT's integration sphere, showing the bottom surface that comes in contact with the sediment.

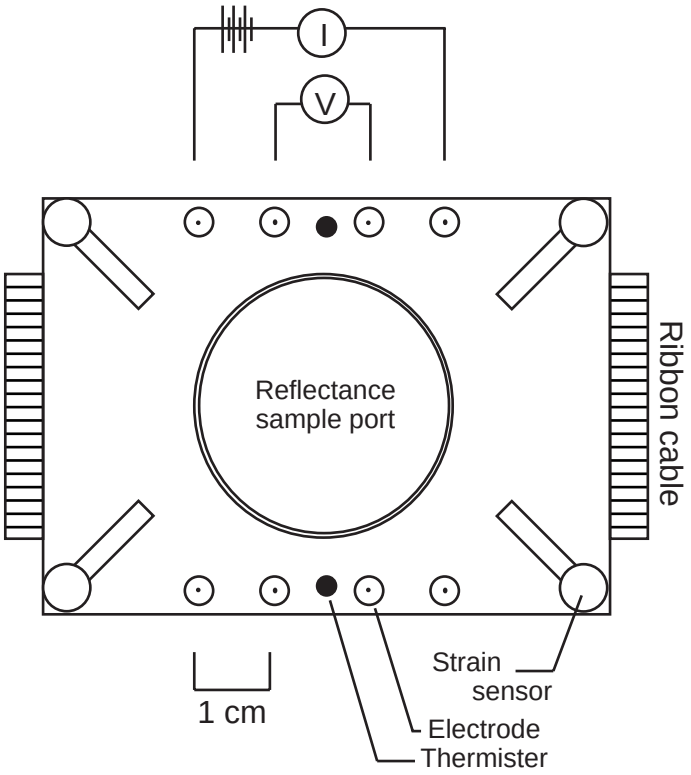

Table T1. Calcareous nannofossil datums used during Leg 177 and their assigned age estimates. (Continued on next page.)

Event	Age (Ma)	Reference	Martini (1971) base	Okada and Bukry (1980) base
FO *E. huxleyi* acme	0.085	1	NN21b	
FO *E. huxleyi*	0.26	1	NN21a	CN15
LO *G. caribbeanica* acme	0.26	2		
LO *P. lacunosa*	0.46	1	NN20	CN14b
LO *R. asanoi*	0.88	3		
RE *Gephyrocapsa* medium	0.96	4		CN14a?
FO *R. asanoi*	1.08	3		
LO *Gephyrocapsa* large	1.24	4		
FO *Gephyrocapsa* large	1.46	4		
LO *C. macintyrei*	1.60	4		
FO *Gephyrocapsa* medium	1.69	4		CN13b?
Pliocene/Pleistocene	1.77			
LO *D. brouweri*	1.95	4	NN19	CN13a
FCO *D. triradiatus*	2.15	4		
LO *D. pentaradiatus*	2.45	5	NN18	CN12d
LO *D. surculus*	2.55	6	NN17	CN12c
LO *D. tamalis*	2.83	6	CN12b	
early/late Pliocene	3.58			
LO *Sphenolithus* spp.	3.66	7		
LO *R. pseudoumbilicus*	3.66	7	NN16	CN12a
FO *P. lacunosa*	4.00	8		
Miocene/Pliocene	5.32			
LO *D. quinqueramus*	5.54	9	NN12	CN10a
LO *A. amplificus*	5.99	9		
FO *A. amplificus*	6.84	9		
FO *Amaurolithus* spp.	7.39	9		CN9b
FO *D. quinqueramus*	8.60	10	NN11	CN9a
FO *D. loeblichii*	8.70	10		CN8b
LO *D. hamatus*	9.63	9	NN10	CN8a
FO *D. hamatus*	10.47	9	NN9	CN7
LO *C. miopelagicus*	10.94	9		
middle/late Miocene	11.20			
LO *C. nitescens*	12.10	7		
FO *C. macintyrei*	12.30	7		
LO *C. premacintyrei*	12.70	7		
LCO *C. floridanus*	13.20	7		
early/middle Miocene	16.40			
FO *C. premacintyrei*	17.40	11		
LO *S. belemnos*	18.30	10	NN4	
FO *D. druggii*	23.20	10	NN2	CN1c
Oligocene/Miocene	23.80			
LO *R. bisecta*	23.90	10	NN1	CN1a
LO *Z. bijugatus*	24.50	10		
LO *C. altus*	26.10	10		
LO *R. umbilica*	31.30	10	NP23	CP18
LO *I. recurvus*	31.8-33.1	10		
Acme *Clausicoccus* spp.	33.30	10		
LO *R. oamaruensis*	33.70	10		
Eocene/Oligocene	33.80			
LO *D. saipanensis*	34.2-35.4	10	NP21	CP16a
LO *R. reticulata*	36.10	10		
FO *R. oamaruensis*	35.40	10		
FO *I. recurvus*	36.00	10	NP19	
FO *C. oamaruensis*	37.00	10	NP18	CP15
LO *C. grandis*	37.10	10		
FO *R. bisecta*	38.00	10		
LO *C. solitus*	40.40	10	NP17	CP14b
FO *R. reticulata*	42.00	10		
LO *N. fulgens*	43.10	10		
LO *B. gladius*	43.40	10	NP16	
FO *R. umbilica*	43.70	10		CP14a
LO *C. gigas*	44.50	10		CP13c
FO *C. gigas*	46.10	10		CP13b
FO *N. fulgens*	47.30	10	NN15	CP13a
FO *D. sublodoensis*	49.70	10	NP14	CP12

Table T1 (continued).

Event	Age (Ma)	Reference	Martini (1971) base	Okada and Bukry (1980) base
LO *T. orthostylus*	50.60	10	NP13	
FO *D. lodoensis*	52.85	10	NP12	CP10
Transition *T. contortus-T. ortostylus*	53.61-54.37	10	NP11	CP9b
Paleocene/Eocene	53.4			

Notes: FO = first occurrence, LO = last occurrence, FCO = first common occurrence, LCO = last common occurrence, RE = reentrance. Zonal codes are those of Martini (1971) and Okada and Bukry (1980). References: 1 = Thierstein et al. (1977), 2 = Pujos (1988), 3 = Wei (1993), 4 = Raffi et al. (1993), 5 = Lourens et al. (1996), 6 = Tiedemann et al. (1994), 7 = Raffi and Flores (1995), 8 = Gartner (1990), 9 = Backman and Raffi (1997), 10 = Berggren et al. (1995b), 11 = Gartner (1992).

Table T2. Planktic foraminifer Subantarctic zonal scheme (Jenkins and Srinivasan, 1986).

Epoch		Subantarctic zonal scheme	Zonal marker
Pleistocene		*G. truncatulinoides*	
			G. truncatulinoides FA
		G. inflata	
Pliocene			*G. inflata* FA
		G. puncticulata	
			G. sphericonomiozea LA
		G. sphericonomiozea	
			G. conomiozea LA
	late	*G. conomiozea*	
			G. conomiozea FA
		G. miotumida	
Miocene			*G. mayeri* LA
		G. mayeri	
			G. peripheroronda LA
		G. peripheroronda	
	middle		*G. conica* LA
		G. conica	
			G. conica FA
		P. glomerosa curva	
			G. miozea (change from random to sinistral coiling)
	early	*G. miozea*	

Notes: FA = first appearance; LA = last appearance.

Table T3. Age assignments of biostratigraphic diatom zones used during Leg 177.

Zone	Reference	Top (Ma)	Base (Ma)
Thalassiosira lentiginosa Subzone c	1	0.00	0.18
Thalassiosira lentiginosa Subzone b	1	0.18	0.42
Thalassiosira lentiginosa Subzone a	1	0.42	0.65
Actinocyclus ingens Subzone c	1	0.65	1.07
Actinocyclus ingens Subzone b	1	1.07	1.30
Actinocyclus ingens Subzone a	1	1.30	1.80
Proboscia barboi	1	1.77	2.00
Thalassiosira kolbei/Fragilariopsis matuyamae	1	2.00	2.50
Thalassiosira vulnifica	1	2.50	2.63
*Thalassiosira insigna**	2	2.63	3.26
Fragilariopsis interfrigidaria	2	3.26	3.80
Fragilariopsis barronii	2	3.80	4.44
Thalassiosira inura	2	4.44	4.92
Thalassiosira oestrupii	2	4.92	5.56
*Fragilariopsis reinholdii**	2	5.56	8.10
Actinocyclus ingens var. *ovalis*	2	8.10	8.68
Thalassiosira torokina	2	8.68	9.01
Asteromphalus kennettii	2	9.01	10.23
Denticulopsis hustedtii	2	10.23	10.63
Denticulopsis dimorpha	2	10.63	11.67
Denticulopsis dimorpha/Nitzschia denticuloides	2	11.67	12.20
Denticulopsis praedimorpha	2	12.20	12.84
Nitzschia denticuloides	2	12.84	13.51
Denticulopsis hustedtii/Nitzschia grossepunctata	2	13.51	14.17
Actinocyclus ingens var. *nodus*	2	14.17	14.38
Nitzschia grossepunctata	2	14.38	15.38
A. ingens/D. maccollumii	2	15.38	16.20
Denticulopsis maccollumii	2	16.20	16.75
Crucidenticula kanayae	2	16.75	17.72
Thalassiosira fraga	2	17.72	20.79
Thalassiosira spumellaroides	2	20.79	22.58
Rocella gelida	2	22.58	26.50
Lisitzinia ornata	2	26.50	27.95
Azpeitia gombosii	2	27.95	28.35
Rocella vigilans	2	28.35	30.24
Cavitatus jouseanus	2	30.24	30.62
Rhizosolenia gravida/oligocaenica	2	30.62	33.22

Notes: * = revised zones. References: 1 = Gersonde and Bárcena (1998), 2 = Gersonde et al. (1998).

Table T4. Compilation of diatom species ranges. (Continued on next page.)

LO (Ma)	FO (Ma)	Species	Reference	Area
6.7	11.05	*A. fryxellae*	2	Southern Ocean
21.1	28.35	*A. gombosi*	4	Southern Ocean
0.64	16.2	*A. ingens*	2	Southern Ocean
12.71	14.38	*A. ingens* var. *nodus*	2	Southern Ocean
6.27	8.68	*A. ingens* var. *ovalis*	4	Southern Ocean
6	10.23	*A. kennettii*	2	Southern Ocean
0	19.05	*A. tabularis* group	2	Southern Ocean
30.8?	34.0?	*Asterolampra punctifera*	2	Southern Ocean
4.89	8.68	*C. intersectus*	3	Southern Ocean
16.56	17.72	*C. kanayae*	4	Southern Ocean
13.2	28.2	*C. lewisianus*	2	Southern Ocean
28.2	28.5	*C. lewisianus* var. *levis*	2	Southern Ocean
28.2?	34.0?	*C. superbus*	2	Southern Ocean
14.61	30.62	*Cavitatus jouseanus*	2	Southern Ocean
15.2?	30.3?	*Cavitatus linearis*	2	Southern Ocean
31.5?	34.0?	*Cestodiscus antarcticus*	4	Southern Ocean
22.3?	30.7?	*Cestodiscus kugleri*	2	Southern Ocean
10.7	12.2	*D. dimorpha*	4	Southern Ocean
5.3	14.17	*D. hustedtii*	2	Southern Ocean
9.80?	16.2?	*D. lauta*	2	Southern Ocean
14.7	16.75	*D. maccolumii*	2	Southern Ocean
11.53	12.4	*D. praedimorpha*	4	Southern Ocean
4.48	8.6	*F. arcula*	2	Southern Ocean
4.18	10.21?-8.75	*F. aurica*	2	Southern Ocean
1.4	4.44	*F. barronii*	2	Southern Ocean
4.3	7.55	*F. cylindrica*	5	Equatorial Pacific
0.00	1.90	*F. doliolus*	5	Equatorial Pacific
0.90	9.00	*F. fossilis*	5	Equatorial Pacific
2.63	3.8	*F. interfrigidaria*	2	Southern Ocean
0	2.70?	*F. kerguelensis*	2	Southern Ocean
2.9	4.62	*F. lacrima*	3	Southern Ocean
2.1	2.5?	*F. matuyamae*	1	Northern Southern Ocean
4.15	11.05	*F. praecurta*	2	Southern Ocean
3.8	5.3	*F. praeinterfrigidaria*	2	Southern Ocean
0.65	8.10	*F. reinholdii*	5	Equatorial Pacific
2.65	3.4	*F. weaveri*	4	Southern Ocean
24	28.0?	*Hemiaulus* sp. *A*	2	Southern Ocean
24.3	27.95	*L. ornata*	4	Southern Ocean
9.8	13.9	*N. claviceps*	2	Southern Ocean
11.7	13.51	*N. denticuloides*	2	Southern Ocean
13.51	15.38	*N. grossepunctata*	2	Southern Ocean
14.61	20	*N. maleinterpretaria*	2	Southern Ocean
1.80	12.50	*P. barboi*	FO: 6, LO: 1	Southern Ocean
18.28	34.0?	*P. praebarboi*	2	Southern Ocean
22.46	26.5	*R. gelida*	2	Southern Ocean
2.90?	4.7	*R. heteropolara*	3	Southern Ocean
30.94	33.22	*R. oligocaenica*	4	Southern Ocean
21.2?	30.3?	*R. praenitida*	2	Southern Ocean
19.4	24.62	*R. symmetrica*	4	Southern Ocean
25.5	28.1	*R. vigilans* (large form)	2	Southern Ocean
28.8	30.24	*R. vigilans* (small form)	2	Southern Ocean
30.5?	34.0?	*Stictodiscus kittonianus*	2	Southern Ocean
2.5	4.44	*T. complicata*	2	Southern Ocean
2.18	3.70	*T. convexa*	5	Equatorial Pacific
2.18	6.70	*T. convexa* var. *aspinosa*	5	Equatorial Pacific
0.7	1.77?	*T. elliptipora*	FO: 6, LO: 1	Southern Ocean
0.70	4.50	*T. fasciculata*	1	Southern Ocean
18.28	20.9	*T. fraga*	2	Southern Ocean
2.63	3.40?	*T. insigna*	4	Southern Ocean
2.5	4.92	*T. inura*	2	Southern Ocean
2	3.75?	*T. kolbei*	4	Southern Ocean
6.27	6.3	*T. miocenica*	4	Southern Ocean
0	5.56	*T. oestrupii*	2	Southern Ocean
19	22.58	*T. spumellaroides*	2	Southern Ocean
1.5	>2.2	*T. tetraoestrupii* var. *reimeri*	7	Northern Southern Ocean

Table T4 (continued).

LO (Ma)	FO (Ma)	Species	Reference	Area
1.8	9.01	*T. torokina*	4	Southern Ocean
2.5	3.26	*T. vulnifica*	4	Southern Ocean
24.0?	34.0?	*Thalassiosira* sp.1 (Fenner, 1978)	2	Southern Ocean

Notes: LO = last occurrence, FO = first occurrence. References: 1 = Gersonde and Bárcena (1988), 2 = Gersonde et al. (1998), 3 = Gersonde and Burckle (1990), 4 = Barron and Baldauf (1995), 5 = Barron (1992), 6 = Harwood and Maruyama (1992), 7 = R. Gersonde (unpubl. data).

Table T5. Ages of biostratigraphically useful radiolarian datums calibrated to the Berggren et al. (1995b) geomagnetic polarity time scale.

Datum	Age (Ma)	Source
LO *Stylatractus universus*	0.46	Caulet, 1991
LO *Pterocanium trilobum*	0.83	Lazarus, 1992
LO *Eucyrtidium calvertense*	1.92	Lazarus, 1992
LO *Triceraspyris antarctica*	1.92	Lazarus, 1992
FO *Lithelius nautiloides*	1.93	Caulet, 1991
FO *Triceraspyris antarctica*	1.93	Caulet, 1991
LO *Helotholus vema*	2.42	Lazarus, 1992
LO *Desmospyris spongiosa*	2.44	Lazarus, 1992
FO *Cycladophora davisiana*	2.61	Lazarus, 1992
LO *Prunopyle titan*	3.5	Lazarus, 1992
FO *Helotholus vema*	4.57	Lazarus, 1992
LO *Helotholus praevema*	4.6-4.62	Caulet, 1991
FO *Desmospyris spongiosa*	4.98-5.01	Caulet, 1991
FO *Prunopyle titan*	5.01-5.11	Caulet, 1991
LCO *Lychnocanoma grande*	5.03	Lazarus, 1992
LO *Amphymenium challengerae*	6.1	Lazarus, 1992
FO *Amphymenium challengerae*	6.58	Lazarus, 1992
FO *Lamprocyrtis heteroporos*	6.79	Morley and Nigrini, 1995
FO *Acrosphaera? labrta*	7.71	Lazarus, 1992
LO *Cycladophora spongothorax*	9.12	Lazarus, 1992
LO *Stichocorys peregrina*	9.22	Lazarus, 1992
LCO *Ceratocyrtis stigi*	9.32	Lazarus, 1992
FCO *Ceratocyrtis stigi*	9.83	Lazarus, 1992
FO *Acrosphaera australis*	10.36	Lazarus, 1992
LO *Cycladophora humerus*	10.53	Lazarus, 1992
FO *Eucyrtidium pseudoinflatum*	10.61	Lazarus, 1992
LO *Actinomma glownini*	10.77	Lazarus, 1992
FO *Cycladophora spongothorax*	12.55	Lazarus, 1992
FO *Dendrospyris megalocephalis*	12.68	Lazarus, 1992
FO *Actinomma glownini*	13.61	Lazarus, 1992
FO *Cycladophora humerus*	14.18	Lazarus, 1992
FO *Eucyrtidium punctatum*	17.02	Lazarus, 1992
FO *Cycladophora golli regipileus*	19.11	Lazarus, 1992
FO *Cyrtocapsella longithorx*	20.72	Lazarus, 1992
FO *Cyrtocapsella tetrapera*	22.48	Harwood et al., 1992
LO *Lithomelissa sphaerocephalis*	23.353-24.730	Takemura and Ling, 1997
FO *Cycladophora campanula*	23.94-25.26	Caulet, 1991
FO *Lipmanella hister*	23.94-25.26	Caulet, 1991
LO *Axoprunum irregularis*	24.118-?28.745	Takemura and Ling, 1975
LO *Eucyrtidium antiquum*	26.77-30.05	Caulet, 1991
LO *Lophocyrtis longiventer*	26.77-30.05	Caulet, 1991
FO *Calocyclas* sp. A	?28.283-29.401	Takemura and Ling, 1997
LO *Lithomelissa challengerae*	?28.283-29.401	Takemura and Ling, 1997
FO *Lychnocanoma conica*	28.745-30.098	Takemura and Ling, 1997
LO *Calocyclas* cf. *semipolita*	30.479-?33.058	Takemura and Ling, 1997
FO *Axoprunum irregularis*	30.939-34.655	Takemura and Ling, 1997
FO *Eucyrtidium antiquum*	30.939-34.655	Takemura and Ling, 1997
LO *Eucyrtidium spinosum*	30.939-34.655	Takemura and Ling, 1997

Note: FO = first occurrence, LO = last occurrence, FCO = first common occurrence, LCO = last common occurrence.

Table T6. Control measurements of thermal conductivity in red rubber.

Site	Thermal conductivity (W/[m·K])	Start (s)	Length (s)
1088			
	0.891	88.0	25.0
	0.853	67.5	27.5
	0.882	118.0	26.0
	0.848	41.5	27.0
1092			
	0.859	74.0	25.0
	0.861	87.0	25.0
	0.915	108.0	25.0
	0.863	95.0	25.5
1093			
	0.892	102.0	27.5
	0.848	52.0	36.5
1094			
	0.871	124.0	25.5
	0.856	46.5	25.0
	0.873	75.5	26.0
	0.890	118.0	25.0
	0.865	69.5	30.5
	0.870	110.0	26.5
	0.884	124.5	25.5
	0.875	79.0	25.5
	0.870	108.5	27.5
	0.869	109.5	26.0
	0.863	73.5	25.0
	0.866	71.0	25.5
	0.882	118.5	25.0
	0.871	88.5	25.0
	0.865	75.0	25.0
	0.864	72.0	25.0
	0.846	45.5	26.5
	0.877	95.0	29.0
	0.866	70.0	26.0
	0.857	57.5	26.0
	0.861	65.5	28.0
	0.863	75.5	26.0
	0.882	121.0	26.0
	0.880	117.5	30.5
	0.872	68.0	27.0
	0.889	109.5	25.5
	0.856	54.5	25.0
	0.886	113.0	25.5
	0.880	114.5	25.0
	0.843	39.5	25.0
Average:	0.870		
St. dev.:	0.014		
St. dev. (%):	1.7		

Notes: St. dev. = standard deviation. This table is also available in ASCII format in the **TABLES** directory.

Table T7. Specifications of the downhole tools deployed during Leg 177.

Tool string	Tool	Measurement	Sample interval (cm)	Depth of investigation (cm)	Approximate vertical resolution (cm)
Triple combination	HNGS	Natural gamma ray	15	Variable	45
	APS	Porosity	5 or 15	15	15-30
	HLDS	Bulk density, PEF	2.5 or 15	15-60	15-45
	DIT	Resistivity	2.5 or 15	38/76/150	59/150/200
GHMT	NGT	Natural gamma ray	15	Variable	45
	NMRT	Total magnetic field	5	Variable	15-30
	SUMT	Magnetic susceptibility	5	Variable	15-30

Notes: Tool abbreviations: HNGS = hostile environment natural gamma-ray sonde, APS = accelerator porosity sonde, HLDS = hostile environment litho-density sonde, DIT = dual induction tool, GHMT = geologic high-resolution magnetic tool, NGT = natural gamma-ray spectrometry tool, NMRT = nuclear magnetic resonance tool, SUMT = susceptibility magnetic tool. PEF = photoelectric factor.